Silicon-Based Integrated Label-Free Optofluidic Biosensors: Latest Advances and Roadmap

Jiawei Wang,* Mariana Medina Sanchez, Yin Yin, Raffael Herzer, Libo Ma,* and Oliver G. Schmidt

By virtue of the well-developed micro- and nanofabrication technologies and rapidly progressing surface functionalization strategies, silicon-based devices have been widely recognized as a highly promising platform for the next-generation lab-on-a-chip bioanalytical systems with a great potential for point-of-care medical diagnostics. Herein, an overview of the latest advances in silicon-based integrated optofluidic label-free biosensing technologies relying on the efficient interactions between the evanescent light field at the functionalized surface and specifically bound analytes is presented. State-of-the-art technologies demonstrating label-free evanescent wave-based biomarker detection mainly encompass three device configurations, including on-chip waveguide-based interferometers, microring resonators, and photonic-crystal-based cavities. Moreover, up-to-date strategies for elevating the sensitivities and also simplifying the sensing processes are discussed. Emerging laboratory prototypes with advanced integration and packaging schemes incorporating automatic microfluidic components or on-chip optoelectronic devices lead to one significant step forward in real applications of decentralized diagnostics. Besides, particular attention is paid to currently commercialized label-free optical bioanalytical models on the market. Finally, the prospects are elaborated with several research routes toward chip-scale, low-cost, highly sensitive, multi-functional, and user-friendly bioanalytical systems benefiting to global healthcare.

Dr. J. Wang, Dr. M. M. Sanchez, Dr. Y. Yin, R. Herzer, Dr. L. Ma
Institute for Integrative Nanosciences
Leibniz IFW Dresden
Dresden 01069, Germany
E-mail: jiawei.wang@ifw-dresden.de; l.ma@ifw-dresden.de
Dr. J. Wang, Prof. O. G. Schmidt
Material Systems for Nanoelectronics
Technische Universität Chemnitz
Chemnitz 09107, Germany
Dr. J. Wang, Prof. O. G. Schmidt
Research Center for Materials
Architectures and Integration of Nanomembranes
Technische Universität Chemnitz
Rosenbergstrasse 6, Chemnitz 09126, Germany

The ORCID identification number(s) for the author(s) of this article can be found under https://doi.org/10.1002/admt.201901138.

1. Introduction

Advancing medical diagnostic technologies is crucial for identifying or preventing human disease in the early stages and performing effective clinical treatments. Nowadays, most of the diagnoses are conducted based on standard tests in centralized clinical laboratories with delicate and sophisticated instruments by well-trained experts. In recent years, personalized medicine has been proposed as a paradigm shift in individualized therapies, featuring monitored progress, evaluated safety, and improved efficiency. Notably, the concept of "point-of-care (POC)" diagnostics emerges with tremendous advances in compact, cost-effective, and reliable bioanalytical systems providing diagnostic testing in a very short time without sophisticated protocols.[1–3] Thus, POC diagnostics for personalized medicine is highly promising for revolutionizing global healthcare at the dawn of the twenty-first century.[4]

Among a large variety of medical diagnostic routes, discrimination and quantification of specific biomarkers in biological fluids have been known as the highly efficient way to trace the corresponding diseases. In the past 40 years, the commercial enzyme-linked immunosorbent assay (ELISA) serves as a standard method of biomarker detection for in vitro diagnostics.[5] However, as a fluorescence labeling-based approach, it has the following limitations: i) need of sophisticated reagent selection and pairing; ii) complex, bulky setup for data readout, and iii) long preparation and operation time. As a consequence, label-free biosensing approaches become desirable to meet the demands of POC diagnostics. Surface plasmon resonance (SPR)-based biosensors are the most well-known and widely applied label-free optical bioanalytical tools since the first successfully commercialized product by Biacore 30 years ago.[6,7] Since then, numerous efforts on label-free optical biosensors have been invested,[8] which cover different types of optical measurements such as transmission,[9,10] emission,[11] adsorption,[12] polarimetry,[13] and light scattering.[14] These sensing techniques reveal potential applications not only in medical diagnostics but also in drug discovery,[15] food safety,[16,17] and environmental monitoring.[18]

Over the past decades, different miniaturized architectures fabricated on a chip have been continuously explored in various

**ADVANCED
SCIENCE NEWS**

www.advancedsciencenews.com

**ADVANCED
MATERIALS
TECHNOLOGIES**

www.advmattechnol.de
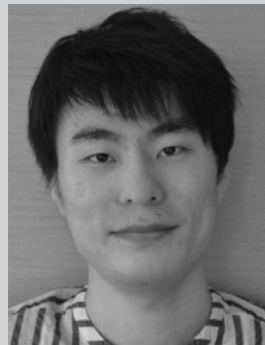
material platforms for label-free optical biodetection, with the common target of pushing the limit of detection (LOD), namely the lowest quantity of a substance that can be distinguished from the absence with a certain confidence level. **Figure 1** summarizes the state-of-the-art chip-scale label-free optical biodetection schemes. Planar film-based schemes mainly include SPR, dual-polarization interferometry (DPI),[19,20] and reflectometric interference spectroscopy (RIfS).[21,22] However, these schemes usually provide only moderate sensing performance (typical LOD down to nanomolar), and hence secondary signal amplifications might be necessary for further optimizations. In the past two decades, shaping metals or dielectric materials into novel micro- and nanoscale structures offer plenty of fresh insights for optical biosensing and push the LODs down to the sub-femtomolar level. In particular, single-molecule detection has been achieved based on techniques such as surface-enhanced Raman scattering (SERS),[23,24] localized surface plasmon resonance (LSPR),[25,26] and ultra-high Q optical microcavities.[27,28]

Silicon and silicon-based materials, typically including silicon nitride (SiN) and silica, are highly appealing for developing integrated optical biosensors in the micro- and nanoscale. In particular, silicon photonics technology is opening a new era and revolutionizing the modern optoelectronics and photonics industries with its unique advantages of mature micro/nanofabrication processes,[29] especially complementary metal-oxide-semiconductor (CMOS)-compatible techniques. The capability of on-chip lightwave guiding in photonic integrated circuits (PICs) and confinement within a compact footprint enables closely interacting with analytes of interest and therefore sensitive biodetection in real-time. Besides, the maturing optofluidic integration techniques shed light on POC tests with simultaneous multiplexed detection for multiple targets, automatic sample processing on a single chip, and a minimized requirement of off-chip components. In this review paper, the latest progress of label-free optically passive biosensing devices integrated on a silicon chip utilizing optical waveguiding and evanescent field-based detection principles is discussed, which mainly involves three types of transducers, namely on-chip

Jiawei Wang received his B.S. degree from Sun Yat-sen University in 2011. He obtained his Ph.D. degree from the Hong Kong University of Science and Technology in 2016. Currently, he is a postdoctoral researcher at Leibniz IFW Dresden and a research associate in the Chemnitz University of Technology working with Prof. O. G. Schmidt. His research interests include optical microcavities, integrated photonics, plasmonics, optofluidics, and optical biosensing.
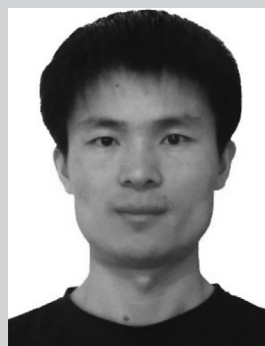
Libo Ma is a research group leader in the Institute of Integrative Nanosciences at Leibniz IFW Dresden. He received his B.S. degree in physics from Shandong Normal University in 2001. He obtained his Ph.D. degree from the Institute of Physics, Chinese Academy of Sciences in 2007. His current research interests include cavity photonics, plasmonics, light–matter interactions, on-chip photonic integration, and topological photonics.

Oliver G. Schmidt has been the director of the Institute of Integrative Nanosciences at Leibniz IFW Dresden since 2007. He holds a full professorship for Materials Systems for Nanoelectronics at Chemnitz University of Technology, Germany. His interdisciplinary activities bridge across several research fields, ranging from nanophotonics and nanoelectronics to materials design and system engineering. His special interest lies with nanomembrane materials which can be strain-engineered and employed in multifunctional devices both on and off the chip.

Figure 1. Summary of chip-scale label-free optical biosensing schemes.

interferometers, microring resonators, and photonic-crystal (PhC)-based cavities. This review article does not cover some other silicon micro/nanostructure-based biosensors displayed in Figure 1 such as resonant gratings[30] and metasurfaces[31,32] in which the optical waveguides and PICs are not incorporated. Furthermore, the latest laboratory prototype systems toward next-generation POC applications are highlighted, which indicates clear technological advances compared with currently

Table 1. Optical properties of common materials involved in the silicon photonics technology.

Materials	Silicon	Silicon nitride (Stoichiometric Si_3N_4 as an example)	Silicon dioxide
Bandgap	1.12 eV	≈5eV	≈9 eV
Transparency window	1.1 – 9 μm	0.25–8 μm	0.13–3.5 μm
Refractive index @ 600 nm	3.95	≈2.04	≈1.46
Refractive index @ 1550 nm	3.67	≈2	≈1.44
Fabrication process	Crystal material/commercially available SOI wafer	LPCVD/PECVD	Thermal growth, PVD, CVD

PVD, physical vapor deposition; CVD, chemical vapor deposition; LPCVD, low-pressure chemical vapor deposition; PECVD, plasma-enhanced chemical vapor deposition.

commercialized technologies. At last, we discuss the future research directions and development roadmap for silicon-based label-free optical biosensors toward ultimately ultra-sensitive, multi-functional, and portable bioanalytical systems.

2. Silicon Photonics for Label-Free Biosensing

2.1. Silicon-Based Material Platform

Compared to other alternative material platforms for developing PICs and integrated optical sensors, such as polymer,[33,34] aluminum oxide,[35] III-V materials,[36] and lithium niobate,[37] silicon features a high-precision, low-cost, and high-yield device fabrication with good reproducibility owing to the mature CMOS processes.[38,39] **Table 1** summarizes the optical properties of common silicon-based materials. In the silicon-on-insulator (SOI) platform, the top silicon layer with sub-wavelength thickness serves as the optical waveguiding medium for near-infrared (IR) light (mostly at telecommunication band). However, the telecommunication wavelength leads to serious water absorption, which makes it not ideal for biomedical research and applications.

The ultra-wide transparency window from visible to mid-IR renders SiN a versatile option for tremendous emerging applications ranging from 3D PICs,[40] nonlinear photonics[41] to biophotonics.[41–43] The SiN-on-silica platform indicates a sufficiently large refractive index contrast and thus tight optical confinement in compact device footprints. Nowadays, multiple commercial foundry platforms including LioniX's TriPleX,[44] Ligentec's Damascene,[45] IMEC's BioPIX,[46] and the IMB-CNM[46] aim at developing SiN-based integrated photonic technologies with ultra-low propagation loss (<1 dB m^{-1}).[42] In particular, the operation wavelength at the visible or near-IR (<1.1 μm) range naturally takes the advantage of ubiquitous and low-cost light sources such as light-emitting diodes (LEDs) or laser diodes, and readout components such as silicon/germanium-based photodetectors (PDs) or CCD/CMOS cameras.[47] In addition, SiN-based photonic devices reveal a less susceptibility to temperature variation due to its relatively small thermo-optic coefficient compared to silicon,[48] which is advantageous for suppressing the environmental noises and improving the stability in sensing tests.

2.2. Optofluidic Integrations for Silicon-Based Biosensors

As a nascent field integrating micro/nanofluidics and optical/photonic technologies, optofluidics opens up remarkable possibilities for fundamental science and applications.[49,50] For biomedical-related studies, it offers a key route to break new ground on multi-functional "lab-on-a-chip" systems with a small footprint, streamlined protocol, low required sample volume, and ideally high throughput.[51–55]

Various straightforward and convenient methods have been developed for integrating silicon-based materials with microfluidic components.[56] Polydimethylsiloxane (PDMS) as a low-cost, easy-to-use, optically transparent and biocompatible material is popular in the field of micro/nanofluidics with the capability of building complex 3D microfluidic circuits.[57] PDMS can be molded using, for example, SU8-masters,[58] methacrylate-mechanized molds,[59] 3D printed molds[60] (i.e., wax printing channels[61]), among others. It is easy to replicate, by mixing the elastomer and catalyzer, typically in a proportion 10:1, poured it on the respective mold and let it solidify upon an applied temperature (≈60 °C) for a couple of hours. The mechanical and optical properties of PDMS can be tuned by changing the proportion between elastomer and catalyzer, the curing conditions, or by incorporating nanomaterials[62] or other functional powders within the elastomer, prior molding.[63] The PDMS-based microfluidic layer can be permanently bound to silica after oxygen plasma treatment due to hydrogen bonding. A thin layer of ethanol solution between the two surfaces prior to bonding might facilitate the precise alignment between PDMS and the silicon chip under optical microscopy.[64] This integration serves as the most common way to introduce fluidic channels to silicon-based optical biosensors for sample delivery and bioconjugation tasks.[65,66] However, there are some drawbacks of optofluidic integrated biosensing using PDMS-based channels, including non-specific adsorption of hydrophobic molecules,[67] deformation in nonpolar organic solvents (e.g., toluene),[68] and difficulty for unmounting the PDMS layer from the chip due to the irreversible bonding. There are alternatives to reduce unspecific adhesion to the PDMS surface. For example, small molecule proteins such as ethanolamine or casein,[69] or polymers such as polyethylene glycol (PEG)[70] can be applied to cover the PDMS surface prior to detection.

Aside from PDMS, SU-8 as a widely used negative photoresist in microelectronic industries is also commonly employed for microfluidic channels. It is a biocompatible material with good transparency in a wide spectrum range. Owing to the standard lithography process, it offers a precision alignment between the on-chip devices and microfluidic channels.[71] SU-8 channels can be directly patterned onto the sensor surface with high precision at different heights in a single step by using multi-wavelength lithography,[72] in particular when a fine interconnection is required between the fluidic inlet/outlet and

**ADVANCED
SCIENCE NEWS**
www.advancedsciencenews.com

**ADVANCED
MATERIALS
TECHNOLOGIES**
www.advmattechnol.de

the sensor device. As a drawback, SU-8 has to be processed in a cleanroom and several processing steps must be conducted for achieving a multilayer platform that consumes more time in comparison with replicated PDMS platforms.[73] Some other UV curable polymers (e.g., NOA 61, NOA 81) have also been adopted for fabricating microfluidic channels.[74] NOA 63, an optical adhesive, could be used as a substitute to PDMS offering high reproducibility and native hydrophilicity.[75] In addition to polymers, silica-based fluidic channels exhibit good material properties concerning their structural stability, chemical inertness, and a low adsorption rate for ambient molecules.[76,77] Moreover, they can be fabricated rapidly with low cost in a wafer-scale by standard lithography and etching process.

2.3. Surface Functionalization Strategies

In contrast to fluorescence-based detection as indirect measurements using labeled secondary antibodies, label-free optical biosensing essentially derives the native properties of analytes, such as molecular weight, light absorption capability, conformation, among others. For example, for an on-chip optical ridge waveguide, the principle of detection is based on the perturbation of the evanescent field induced by the measured sample. As shown in the numerically simulated transverse magnetic (TM) waveguide mode profile in **Figure 2**a, the light field is confined inside the waveguide core by total internal reflection (TIR) due to the sufficiently large refractive index contrast between the core and surrounding media (i.e., cladding layers and fluid). Notably, the evanescent field penetrates into the surrounding media. The transducer surface is functionalized in order to specifically immobilize the analyte of interests. Any perturbation on the evanescent field due to analyte binding leads to a slightly modified effective refractive index (n_{eff}), and hence can be detected by the output light intensity signals or the transmission spectrum profiles. Therefore, optical label-free biosensing is highly suitable for investigating real-time binding kinetics and accurately quantifying the concentration of an analyte.

Surface functionalization is a wide field of research which makes use of the surface properties of different materials (e.g., metals, oxides, polymers) to allow the immobilization of certain

biomolecules, in particular, bioreceptors, and hence the recognition of the analyte of interest. The reliability and method of biomolecule immobilization is an indispensable step to identify the analyte specifically and selectively, affecting directly the sensitivity, stability, and reproducibility of the sensing device. Surface functionalization and bioconjugation strategies for silicon-based materials and various kinds of biomolecules (e.g., antibodies, peptides, enzymes, nucleic acid sequences, cell receptors) have been widely investigated.[78,79]

The simplest approach adopted in the early studies is the physical adsorption of bioreceptors via hydrophobic and electrostatic interactions. However, it has several fatal drawbacks. First, the non-specific binding results in random orientation of bioreceptors and hence a lack of reproducibility for sensing tests. Second, there is a high risk of undesired folding or desorption of bioreceptors under flow, which increases the uncertainty of sensing results. In contrast to non-oriented and non-uniform binding via physisorption, biochemical functionalization strategies lead to extremely dense and oriented layers of bioreceptors immobilized on the sensor surface, which maximizes the possible binding events and minimizes non-functionalized sites for non-specific binding events. Very well established protocols exist to immobilize biorecognition elements onto different surfaces, in particular on oxides such as SiO_2, Al_2O_3, TiO_2, or metals. Such methods are based either on covalent binding (e.g., amide coupling, silanization, copolymerization), or on non-covalent binding (e.g., π interactions, complexation/chelation, and electrostatic interactions). After immobilizing the bioreceptor, the analyte (e.g., protein, complementary DNA, aptamer, cell) can be recognized and bound to it through different mechanisms.

Figure 2b–d summarizes three main types of biochemical recognition events between the bioreceptor and the analyte, including i) antibody-antigen biorecognition inspired in immunoreactions; ii) hybridization between nucleic acid single strands and the immobilized nucleic acid probe; iii) non-covalent binding between the immobilized active affinity tag and the systems with a known high affinity (e.g., biotin-avidin/streptavidin systems, His-Tag system, Protein A/G for antibodies).

Chemical activation is required for silicon-based materials as the first step, which involves surface oxidation to expose
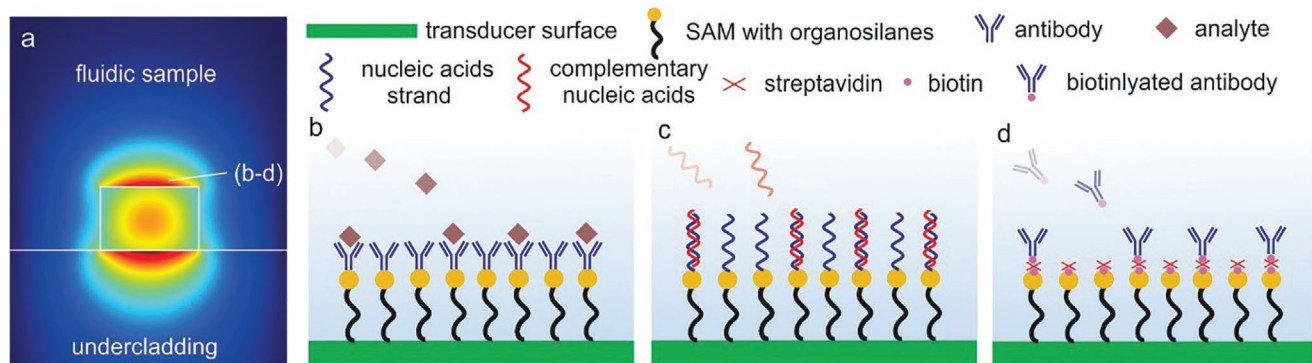
Figure 2. a) A cross-sectional view of the simulated mode field amplitude profile for a SiN optical waveguide at 1550 nm wavelength by COMSOL wave optics module. b–d) Schematic showing three common surface functionalization and binding strategies for silicon-based materials. b) Specific binding between antigens and immobilized antibodies. c) Hybridization between nucleic acids. d) Affinity binding between biotin (as one example of immobilized affinity tags), streptavidin, and the biotinylated antibody.

Table 2. Summary of disease biomarkers existing in body fluids discriminated and quantified by state-of-the-art silicon-based label-free optical biosensing techniques.

Application on diagnostics	Biomarker	Fluid	Receptor/target	Device configuration	Detection limit	Ref.
Acute inflammation	C-reactive protein (CRP)	Serum and plasma	Anti-CRP	Microring	≈200 fM	[92]
Acute inflammation	CRP	Serum	Anti-CRP	BB-MZI	≈2.1 ng mL^{-1}	[93]
Acute inflammation	CRP	Buffer solution	Anti-CRP	BB-MZI	≈19 ng mL^{-1}	[94]
Infections and inflammatory diseases	Cytokines interleukin (IL) 2,4,5	Serum-containing cell media	Anti-IL 2,4,5	Microring	6–100 pM	[95]
Meningitis	Bacterial transfer-messenger RNA (tmRNA)	Buffer solution	Complementary ssDNA	Microring	53 fM	[96]
Tuberculosis	Lipoarabinomannan (LAM)	Urine	Anti-LAM	BB-MZI	≈27 pM	[97]
Tuberculosis	Single-stranded DNA (IS6110)	Sputum	Single-stranded DNA (IS6110 and IS1081)	Microring	5 fg uL^{-1}	[98]
Breast cancer	Human epidermal growth factor receptor 2 (HER2)	Buffer solution	Anti-HER2	Microring	2.5 µg mL^{-1}	[99]
Lung cancer	ZEB1 gene in the lysates	Whole cell lysate	Anti-ZEB1	PhC	1 cell mL^{-1}	[100]
Prostate cancer	Prostate specific antigen (PSA)	Buffer solution	Anti-PSA	Microring	0.4 nM	[101]
Bowel cancer	Carcinoembryonic antigen (CEA)	Serum	Anti-CEA	Microring	10 pM	[102]
Pancreatic cancer	Hepatic growth factor, chemokine ligand 4, fas ligand	Serum	Antibodies (not specified)	PhC	3 fM	[103]
Bladder cancer	2 miRNA	Urine	Complementary DNA	Slot MZI	≈1 nM	[104]
HIV	Human immunoglobulin (Hu-IgG)	Goat serum	Anti-Hu-IgG	Microring	1 ng	[105]

the silanol groups for cross-linking with the organosilanes.[80] For SiN, an etching of the native oxide layer followed by thermal oxidation is favored. To increase the density of reactive hydroxyl (-OH) groups, oxygen plasma or chemical treatment (e.g., using piranha solution) are usually adopted. The activated surface is ready for salinization with the exposed reactive groups susceptible to reaction with specific bioreceptors. Researchers have developed hundreds of organosilanes with different functional groups, such as amino (-NH$_2$), carboxylic (-COOH), and thiol (-SH) for protein/enzyme/nucleic acid binding. As a widely adopted method, (3-Aminopropyl)-triethoxysilane interacting with the surface hydroxyl groups leads to highly stable, oriented self-assembled monolayers covalently bonded on the surface (see Figure 2b). For immobilization of nucleic acid probes in Figure 2c, the incorporation of reactive groups at the end of the nucleic acid sequence is required during the synthesis.[81,82]

Regarding non-covalent affinity binding strategies, one well-established method is based on the biotin-avidin/streptavidin system via a sandwich-like assay (biotin immobilized on the sensor surface/(strep)avidin/biotinylated biomolecule, see Figure 2d).[83] The (strep)avidin-biotin complex is the strongest known non-covalent interaction between a protein and ligand. As a consequence, it is also widely adopted for proof-of-concept demonstrations in optical biosensors.[84,85] Recently, monolayer graphene was utilized by integration on top of silicon microrings for efficiently detection molecule adsorption (e.g., dopamine) by π stacking.[86]

Medical diagnostics requires the identification and quantification of specific disease biomarkers in real biofluids.[87] **Table 2** summarizes currently developed silicon-based

surface-functionalized optical biosensors with demonstrated label-free detection of corresponding biomarkers for disease diagnostics. Notably, complex human biofluid samples (e.g., blood, urine, serum, saliva, sputum, tears, and sweat) contain a large number of other molecules. The potential non-specific binding may lead to a complicated background or false signals.[88] Therefore, blocking the "free" sites without bioreceptors with inert molecules should be implemented for suppressing the occurrence of non-specific binding and hence ensuring sensing with high specificity. Blocking compounds in conventional biosensing tests includes bovine serum albumin,[89] fish gelatin,[90] and Tween 20.[91] However, this method may still face problems for sensing in plasma or serum samples. Functionalizable antifouling coatings have been continuously explored to minimize the non-specific binding and improve sensing accuracy.[88]

3. Silicon-Based Label-Free Optical Biosensors

In this section, we present an overview of the latest achievements on silicon-based label-free optical biosensors. **Figure 3** summarizes four representative photonic structures for evanescent field-based sensing, including Mach–Zehnder interferometer (MZI), bimodal waveguide (BiMW)-based interferometer, microring resonator, and PhC-based cavity. The detailed sensing principles have been clearly explained in previous review articles.[73,106–109] Here we focus on the latest breakthroughs in pushing the sensing performance, extending the functionalities, and simplifying the sensing protocols.
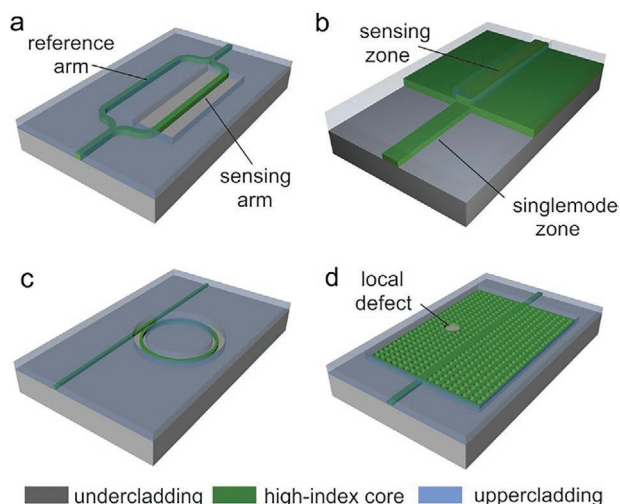
Figure 3. Schematics showing four typical on-chip biosensing structures. a) Mach–Zehnder interferometer, b) BiMW-based interferometer, c) microring resonator, and d) PhC-based resonator.

3.1. On-Chip Interferometer-Based Optical Biosensors

Optical waveguide-based interferometers as on-chip sensors have been extensively investigated since the early 1990s.[110,111] Combining the evanescent field-based sensing principle and on-chip interferometry, the sensors reveal a broad dynamic range and simple readout scheme. The typical interferometer configuration includes Young,[112] Mach–Zehnder,[17,113] Hatman,[114] BiMW-based interferometers,[115] and directional couplers.[116] In particular, MZI and BiMW-based biosensors have been widely exploited in recent years toward medical diagnostic applications.

For MZI-based biosensors in Figure 3a, the two split parts serve as the "sensing" arm and "reference" arm, respectively. The interaction between analyte and evanescent field of the sensing arm results in a phase shift, and consequently changes the interference signals at the output where two arms get combined. A typical MZI-based sensing system only requires a fixed-wavelength laser source and a PD/camera for data readout, which is highly favorable for cost-effective POC diagnostics. In 2015, Si_3N_4 MZI-biosensor arrays were employed for multiplexed detection of microRNAs as potential biomarkers in clinical urine samples of bladder cancer patients.[104] **Figure 4**a displays the key components in such a MZI-based multiplexed biosensing system, including grating couplers for input-coupling of a laser beam at telecom wavelength (inset (i)), strip-slot waveguide mode converters (inset (ii)), sensing arms with a slot-waveguide design to elevate the sensitivity (inset (iii)), and an IR camera for data readout (inset (iv)). The hybridization between the DNA probe and microRNA target can be real-time monitored by the intensity signal changes (inset (v)). Hence the extracted phase change can be correlated with the analyte concentrations over a wide dynamic range. Compared to conventional "asymmetric" MZI-based biosensors with the reference arm under solid cladding, the emerging "symmetric" ones have both arms under liquid environment.[117] In 2016, the symmetric MZI-based biosensors were reported using inkjet technique-enabled localized functionalization of the sensing arm.[117] The experimental results indicate a nice self-referencing property of the symmetric MZI design to environmental noises such as the liquid refractive index change.

However, the conventional MZI operating at a fixed probe wavelength has its inherent shortcomings. The sensitivity is not constant and fades when the signal is around the extreme values of the transmission curve. Besides, the sign of phase change may also cause ambiguities due to the periodicity of transmission profiles. In 2014, Misiakos et al. pioneered the broadband (BB)-MZI-based sensing technology using on-chip waveguide-coupled silicon avalanche LED as the broadband light source.[93,118] As shown in Figure 4b, the output light of such a monolithic integrated sensor chip is coupled through a fiber to an off-chip spectrometer. The sinusoidal output spectrum with a spectral shift can be analyzed using discrete Fourier transform (DFT) so that the phase can be discerned by the argument of the complex DFT value at the main peak. The system has been exploited for detecting C-reactive protein (CRP) which is a common biomarker in human serum samples as an early indicator of ammation and infection. Figure 4b shows the summarized sensor response as the averaged results of ten multiplexed BB-MZI biosensors on a single chip for detecting different CRP concentrations.

Significant breakthroughs on BiMW interferometer-based biosensors have been accomplished by Prof. Laura M. Lechuga's research group in recent years. In Figure 4b, a single BiMW consists of two distinct zones, namely the "single-mode" zone and the "sensing" zone which supports both fundamental and first-order waveguide mode. The fundamental mode reveals a much weaker evanescent field for biointeraction compared to that of the first-order mode.[82] As two modes reveal different n_{eff} and phase velocity, the interference pattern at the output port changes when the bound analyte interacts with two modes. Capture and analysis of bacteria (*Bacillus cereus* and *Escherichia coli*) in ascitic fluids were first reported using BiMW biosensors in 2016 (see Figure 4c).[119] Figure 4d displays the sensor chip equipped with sixteen multiplexed BiMWs. Real-time signal monitoring of bacteria bound to immobilized antibodies and sensor regeneration is shown in Figure 4e. Very recent progress on BiMW biosensors reported identifying and quantifying nosocomial bacteria using specific receptors, which involves a silane-PEG-COOH coating as the bacteria-repelling strategy to avoid extra blocking and reach fast (≈12 min) and accurate detection.[121]

Moreover, Si_3N_4 BiMW biosensors have been applied for quantification of microRNA (miR-181a) with aM concentrations in 2016[115] and human Growth Hormone (hGH) with a LOD down to 10 ng mL^{-1} in 2017,[122] respectively. Both tests were conducted in human urine samples without purification. Real-time specific detection of alternative spliced pre-mRNA as an early-stage indicator of cancers was demonstrated using DNA probe-functionalized sensors.[120] The calibration curve in Figure 4f reveals a clear detection of the specific isoform (Fas 57) and discrimination of the non-complementary isoforms (here Fas 567). The demonstrated sub-pM LOD is three orders of magnitude lower than those achieved by conventional SPR biosensors. However, BiMW biosensors usually have a relatively large footprint, which requires a relatively high sample volume and may limit the possibility of future integrations.
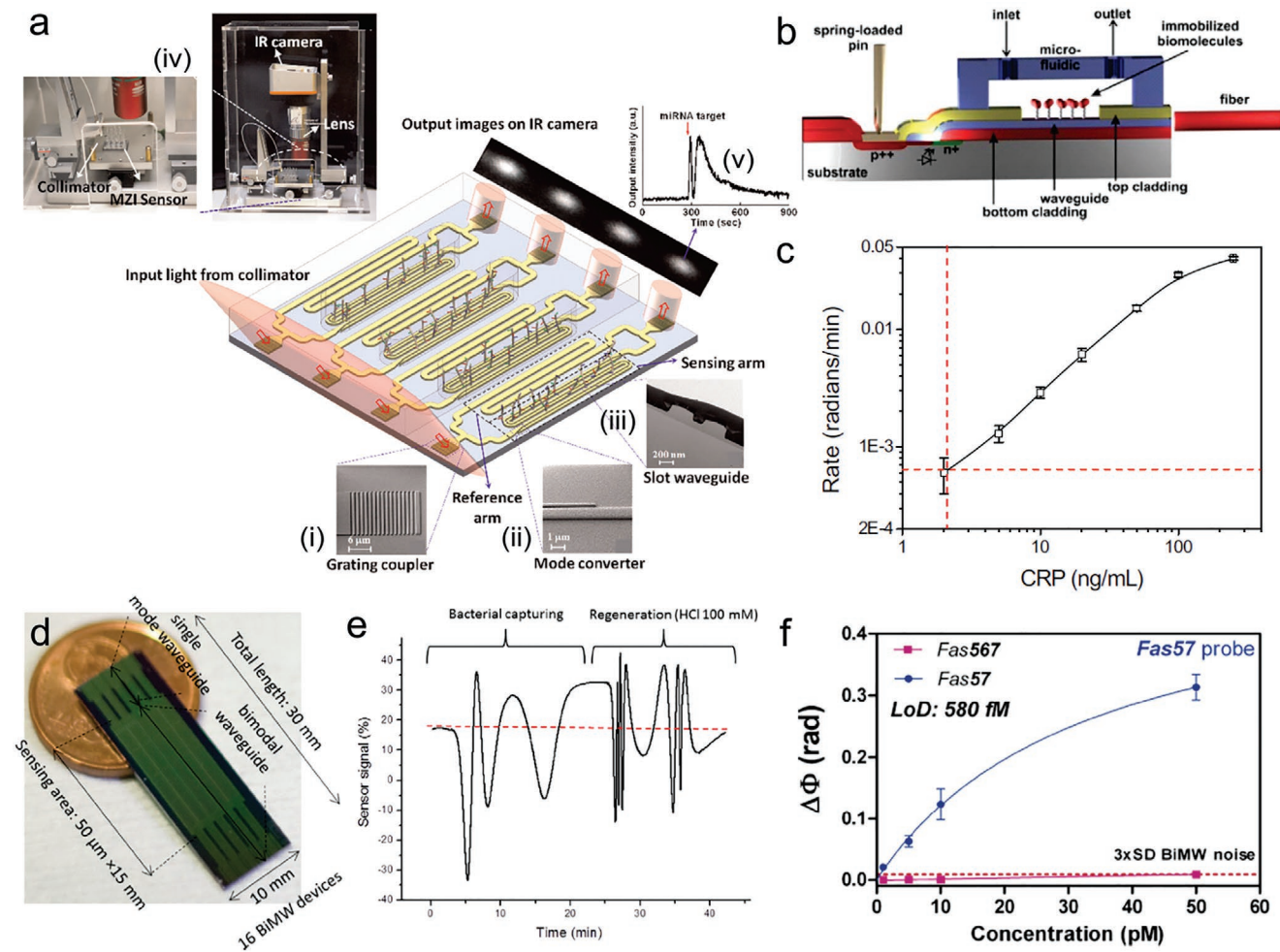
Figure 4. a) Schematic diagram of a silicon MZI biosensing system for microRNA detection. Insets: i) Scanning electron microscopy (SEM) image of the grating coupler, ii) SEM image of the mode converter, iii) Transmission electron microscopy (TEM) image of the slot waveguide region in a cross-sectional view, iv) Picture of the whole experimental setup, v) Measured curve of output intensity showing a ≈4π phase shift. Reproduced with permission.[104] Copyright 2015, Elsevier. b) Schematic showing the cross-sectional view of a BB-MZI sensor integrated with on-chip LED light sources and a microfluidic channel. c) Measured phase change curve as a function of CRP concentration. Red dashed lines indicate the LOD. Reproduced with permission.[93] Copyright 2017, Elsevier. d) Photo of a sensor chip with 16 integrated BiMW biosensors. e) Real-time monitoring of bacteria binding and sensor regeneration process. Reproduced with permission.[119] Copyright 2016, Elsevier. f) BiMW calibration curves of two Fas gene alternative splicing isoforms upon Fas57 probe. The solid line is a nonlinear fit and the dashed line is the noise level (three standard deviations). Reproduced with permission.[120] Copyright 2017, Springer Nature.

3.2. Microring Resonator-Based Optical Biosensors

For circular-shaped dielectric microstructures, the lightwave guided by TIR with multiple round-trips circulating at the cavity boundaries leads to optical resonances, namely whispering-gallery modes (WGMs).[123] In 2002, Vollmer and Arnold first explored WGM microcavity-based biosensing by measuring the spectral shift of WGMs in silica microspheres.[124] For on-chip planar WGM microcavities, such as microrings[84] or microdisks,[125,126] sharp resonances with high quality (Q) factors (defined as the ratio between the resonant wavelength and full width at half-maximum linewidth) typically ≈10^3–10^4 can be obtained within a small device footprint, which potentially gives rise to better discrimination of smaller spectral shift and hence an improved LOD compared to those of waveguide-based interferometers.[127–129] As shown in Figure 3c, the incident light can

be coupled into the microring resonator through a bus waveguide via evanescent coupling. In 2007, De Vos et al. pioneered integrated microring-based biosensors on SOI platform with proof-of-concept demonstrations of detecting biotin-avidin interaction.[84] Later multiplexed sensor arrays of SOI microring resonators have been developed for simultaneous detection of five protein biomarkers[130] and later two DNA oligonucleotide probes[131] in complex media. Protein detection with eight logs of concentration down to the sub-pM level has been experimentally demonstrated.[131] Furthermore, site-selective surface functionalization of multiple microrings by a non-contact "inkjet" method has been developed for multiplexed detection since 2011.[117,132]

In addition to silicon on-chip microring-based biosensors, significant achievements have also been accomplished on SiN-on-silica platform. Ghasemi et al. reported five cascaded SiN
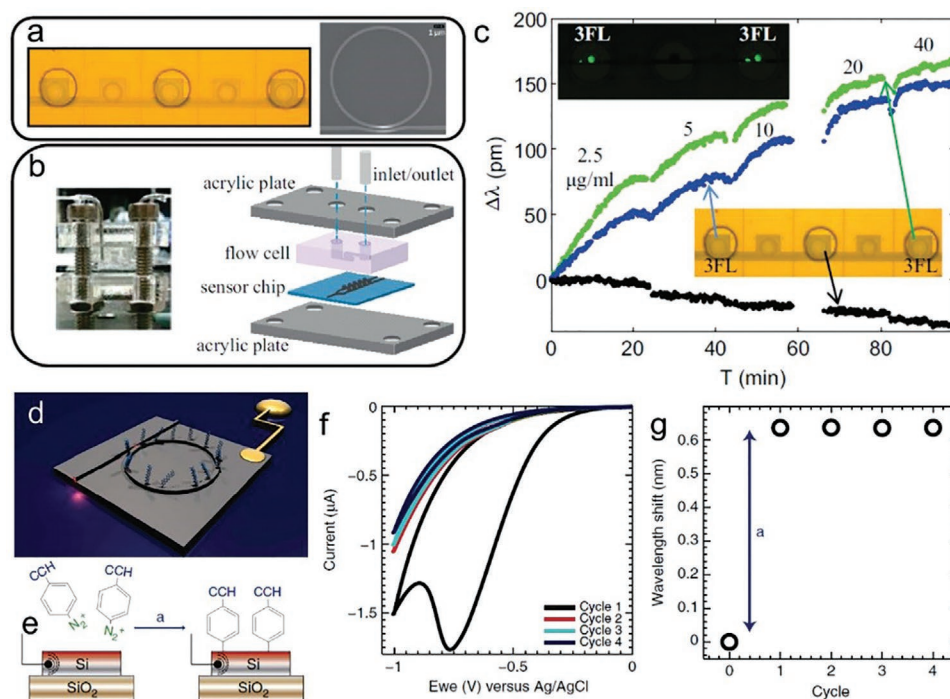
**ADVANCED
SCIENCE NEWS**
www.advancedsciencenews.com

**ADVANCED
MATERIALS
TECHNOLOGIES**
www.advmattechnol.de

Figure 5. a) Optical microscope image of five cascaded SiN microrings and SEM image of one microring. b) Picture of the assembled sensor chip and schematic showing different layers of the optofluidic integrated sensor chip. c) Binding dynamics of AAL to 3-fucosyl lactose (3FL) for two sensing rings (green and blue curves) and one reference ring coated with PEG (black curve). Sensing tests were implemented with the first and last ring functionalized with specific glycans (3FL) and the middle ring with a PEG coating as a reference. Insets: Fluorescence image showing the functionalization of 3FL (upper left) and bright-field image (lower right). Reproduced with permission.[133] Copyright 2016, Elsevier. d) Schematic of a single electrophotonic microring sensor. e) Schematic showing the electrografting process of 4-ethynylbenzene molecules to the silicon photonic electrode. f) Electrochemical response during diazotization and electrografting. g) Measured spectral shift induced by the change of refractive index at the cladding layer. Reproduced with permission.[134] Copyright 2016, Springer Nature.

microring-based biosensors with site-selective functionalization for multiplexed lection detection using a molecular printing system in 2016 (see **Figure 5**a,b).[133] Microrings functionalized with specific glycan for lectin binding suggests minimum nonspecific binding to other lectins. Figure 5c shows the real-time binding curve of biotinylated Aleuria aurantia lectin (AAL) with a clear spectral redshift for two glycan-coated microrings and only a weak response of the reference ring with a PEG coating. For nucleic acid detection, an asymmetric isothermal amplification technique modified based on recombinase polymerase amplification (RPA) was applied to a cascaded microring sensor array in 2017[98] Multiplexed detection of single-stranded DNAs as tuberculosis biomarkers (insertion sequence IS6110 and IS1081) in clinical sputum specimens was performed with a significant spectral shift signal amplification by binding between RPA proteins and the probe or the probe/target complex.

Apart from all-optical microring sensors, the concept of merging silicon-based optical and electrochemical sensors for multi-functional detection was first realized by Juan-Colas et al. in 2016. Optimal n-doped silicon microrings serve as label-free optical sensors with real-time in situ monitoring of electrochemical processes (see Figure 5d).[134,135] By limiting the dopants at a thin layer around the waveguide core, high-Q resonances can be well retained. Figure 5e illustrates the electrochemical modification of the electrode surface. In situ diazotization and electrografting of 4-ethynylbenzene diazonium

were revealed with a clear reduction of the current peak in the first cycle (see Figure 5f). Afterward, a negligible response after the first cycle suggests the complete assembly of a molecular layer. In terms of optical sensing, the spectral shift in Figure 5g confirms the formation of a densely packed molecular layer. Later in 2017, a cascaded electrophotonic microring structure was developed for separate quantifications of refractive index and thickness of molecular layers such as proteins and DNA oligonucleotides.[136]

3.3. On-Chip Photonic Crystal Cavity-Based Optical Biosensors

Usually, an on-chip PhC structure consists of periodically repeating cylindrical air pores in a waveguiding slab layer (see Figure 3d).[137,138] The periodicity of the refractive index profile results in a photonic bandgap (PBG) around the operation wavelength. By introducing a local defect (e.g., missing holes), an optical resonance can be formed as a sharp peak within the bandgap. The resonance with strong optical confinement and minimized mode volume exposed to the environmental media is highly advantageous for detecting tiny perturbation caused by analyte binding.[139,140]

In 2007, Fauchet et al. pioneered the research on silicon 2D PhC cavity-based optical biosensors consisting of a hexagonal array of cylindrical air pores and a central pore with a smaller
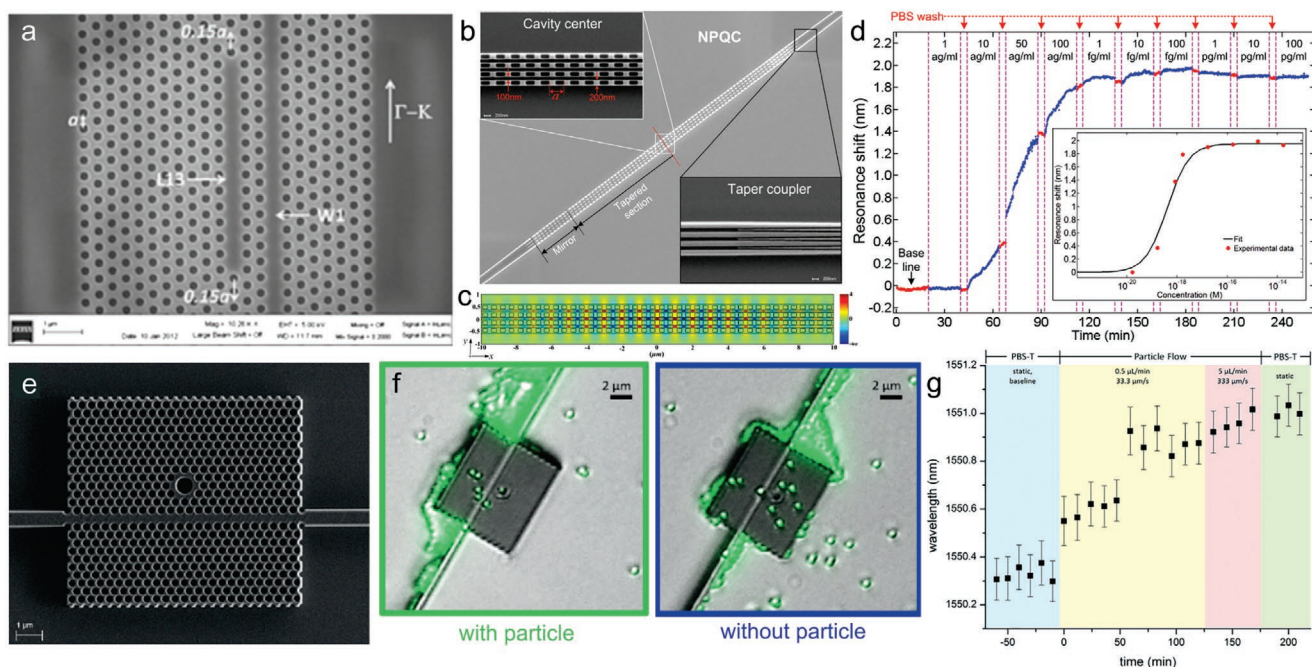
Figure 6. a) SEM image of a fabricated L13 PC microcavity coupled to a W1 PC waveguide. The lattice constant a is 400 nm. Reproduced with permission.[100] Copyright 2013, Elsevier. b) SEM image of a fabricated nanoslotted parallel quadrabeam PhC cavity. Insets: Zoomed-in views at the PhC region and tapered coupler region. c) Simulated electric field distribution of optical resonances using the finite-difference time-domain method. d) Real-time measurement of streptavidin-biotin binding upon various concentrations. Inset: Summarized resonance shift as a function of streptavidin concentration with a fit using Langmuir equation. Reproduced with permission.[143] Copyright 2014, American Institute of Physics. e) SEM image of a 2D PhC cavity-based biosensor with a 585 nm-diameter-large defect hole in the middle region as the sensing site. f) Fluorescence microscopy images showing the 2D PhC with and without the presence of nanoparticle (290 nm-diameter fluorescent latex spheres) at the sensing site. g) Measured resonant wavelength as a function of time for monitoring the interaction between the sensor and virus-simulants. Reproduced with permission.[145] Copyright 2017, Royal Society of Chemistry.

size as the local defect for proof-of-concept demonstration of detecting molecule monolayer binding.[141] In 2013, a line defect-based PhC waveguide-couped cavity was employed by Chakravarty et al. for multiplexed detection of cancer-associated proteins from complex mixtures (ZEB1 in lysates from NCI-H358 lung cancer cells) (see **Figure 6**a).[100] In 2017, the same research group further demonstrated multiplexed PhC-based biosensors with four different defect designs coupled through a 1 × 4 multimode interferometer as an optical splitter, which enables a wide detection range (>5 orders of magnitude for concentrations).[142] Besides, nanoslotted parallel quadrabeam PhC cavities regarded as a precisely tailored 1D PhC design feature simultaneously a high Q factor and large spectral sensitivity, which have been employed for ultra-sensitive detection (see Figure 6b).[143] Numerical simulation results reveal a strong field localization at slotted regions for enhanced interaction with analytes (see Figure 6c). Measurement results in Figure 6d suggest a LOD <10 ag mL^{-1} for streptavidin detection.

In consequence of the much smaller mode volume compared to those of other optical waveguide-based biosensors, PhC-based biosensor is a perfect candidate for detecting discrete nano-sized objects.[144] In 2017, Baker et al. first applied waveguide-coupled 2D SOI PhC sensors for sensitive detection of virus-sized particles under fluidic flow (see Figure 6e).[145] Fluorescence microscopy images in Figure 6f reveal two cases with and without targets at the sensing site, respectively. The real-time detection curve of virus-simulant particles (latex

particles attached to anti-human IgG molecules) under fluidic flow in Figure 6g indicates two discrete jumps as the sign of particle capture. Furthermore, detecting single 20nm-radius polystyrene nanoparticles in aqueous environments was also reported using a slotted PhC as an optimized design.[146]

4. Emerging Sensor Designs and Biosensing Strategies

4.1. Strategies for Improving Sensitivity

Substantial research efforts have been devoted to optimizations of sensor designs for elevating the sensitivity.[147] Various simple, generic yet efficient design rationales have widely demonstrated on different on-chip optical biosensors, including: i) adopting TM-polarized optical modes with strong evanescent fields near the top surface[113,148]; ii) introducing slotted segment at the sensing region[149–154]; iii) designing an ultra-thin (sub-100 nm) waveguide dimension[155]; iv) developing suspended sensing structures to maximize the interaction between evanescent field and analytes[156]; and v) adopting porous silicon as the waveguiding material to boost the active sensing area.[157,158] In this section, we highlight other emerging novel concepts for improving sensitivity in recent years.

Vernier principle which was usually adopted in coupled WGM microcavities for generating single-mode lasing,[159,160]

has also been proved as an efficient sensing scheme using cascaded microrings.[161] The two microrings exhibit slightly different sizes and hence mismatched free spectral ranges, which leads to a periodic envelope function with a peak corresponding to the maximum overlap of individual resonances. A tiny perturbation of one microring is revealed as a giant shift of the main peak in the envelope. Such a data interrogation suggests a tremendous enhancement of sensitivity up to two orders of magnitude.[162–164] However, this method requires wavelength scanning over a very broad range, which largely limits the detection speed.

Another appealing concept is to incorporate conventional solid-core optical waveguides with periodic hole-based PhC structures for biosensing. In 2016, Qin et al. proposed and demonstrated silicon slow-light MZI-based biosensors with the sensing arm integrated with 1D PhCs (see **Figure 7**a–d) for nucleic acid detection.[165] The decreased group velocity leads to enhanced temporal interaction with analyte. Furthermore, the air hole design in Figure 7d results in improved mode spatial overlapping with bound molecules. The characterized phase sensitivity of the slow-light MZI in bulk refractive index sensing tests is five-fold higher than conventional ones. Recently, Uchiyamada et al. reported a bimodal interferometer-based biosensor incorporating a 2D array of holes (see Figure 7e,f) termed "perforated bimodal sensors."[166] Here the 2D sub-wavelength hole array does not show any PBG effect.

The hole sizes are limited to <180 nm to avoid scattering losses. Nevertheless, the strong mode exposure into the surrounding media leads to ≈22-fold enhancement of surface sensitivity compared to a non-perforated bimodal sensor with an equivalent length.

PhC-integrated microring resonators with periodic-patterned holes were first demonstrated in 2012 as slow-light structures for wavelength-division multiplexing applications.[167] In 2017, Lo et al. applied them for label-free biosensing (see Figure 7g).[168] The PBG is engineered around the telecommunication band close to the operation wavelength so that a large group index can be obtained. More than twofold enhancement of bulk sensitivity and spectral shift signals in protein detection were obtained compared to those of conventional solid-core microrings.

Sub-wavelength grating metamaterials emerge as a powerful tool for on-chip light field manipulation,[169] which potentially brings new insights for biosensing.[170–173] Typically, the working mechanism of the 1D sub-wavelength grating (SWG) structure is similar to Bragg gratings or 1D PhCs. However, SWG structures adopted for optical biosensing reveal a much smaller period than that in the Bragg condition to ensure a lossless waveguiding mode. Therefore the mode propagation profile is similar to the common solid-core waveguide. Nonetheless, a large portion of the optical mode extended to the low-index region facilitates the biointeraction. In 2015, Donzella et al. first
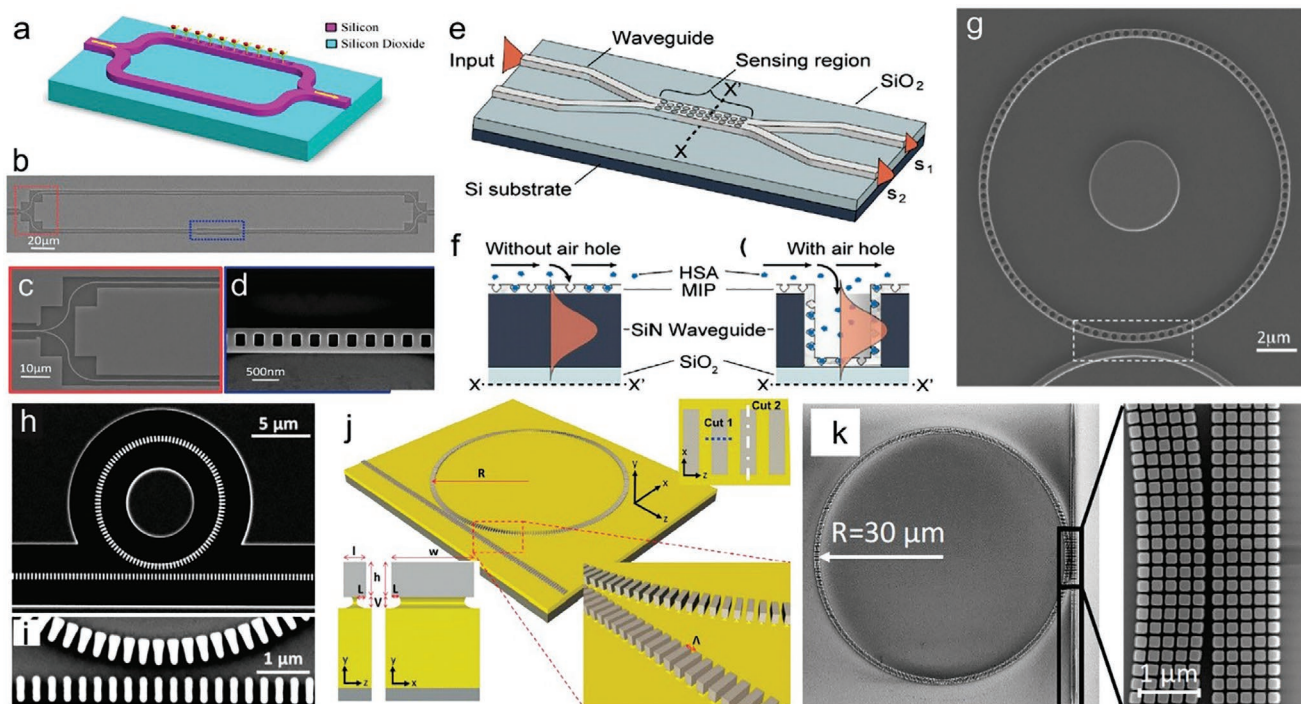

Figure 7. a) Schematic of a slow-light MZI biosensor. b–d) SEM images of b) the fabricated sensor, c) zoomed-in view at the input splitter region, and d) zoomed-in view of the PhC region. Reproduced with permission.[165] Copyright 2016, The Optical Society. e) Schematic of a perforated bimodal interferometer. f) The sensing region in a cross-sectional view for non-perforated (left) and perforated (right) sensors. Reproduced with permission.[166] Copyright 2019, Wiley-VCH. g) SEM image of a fabricated PhC microring. Reproduced with permission.[168] Copyright 2017, The Optical Society. h) SEM image of an SWG microring resonator based on trapezoidal silicon pillars. i) Zoomed-in view of the coupling region. Reproduced with permission.[176] Copyright 2016, The Optical Society. j) Schematic showing pedestal SWG microrings in a perspective view, top view, and side view. Reproduced with permission.[177] Copyright 2019, Elsevier. k) SEM image of a fabricated multi-box microring consisting of five rows of SWG structures. Reproduced with permission.[178] Copyright 2018, The International Society for Optics and Photonics (SPIE).

reported SWG microring with a characterized sensitivity to bulk refractive index change of ≈400 nm per refractive index unit (RIU) which is one order higher than that of common strip waveguide-based microring.[171] Then the SWG microring biosensors were exploited for label-free bio-sandwich assay.[174,175] In 2016, trapezoidal silicon pillar-based SWG microring (see Figure 7h,i) has been reported with mitigated bending losses and ≈3-5 fold enhancement of Q factor,[176] which is envisaged to further improve the sensing performance. In 2019, Chang et al. reported silicon pedestal SWG microrings as ultra-sensitive biosensors (see Figure 7j).[177] The pedestal structure formed by a controlled undercut etching maximizes the mode overlapping with surrounding media. The streptavidin-based bioassay suggests a ≈4-fold enhancement of spectral shift signals compared to that of the control SWG device.

In 2018, Luan et al. proposed and demonstrated a "multi-box" microring biosensor as a fusion of SWG and slot structures (see Figure 7k) with one of the characterized record highest sensitivities to bulk refractive index change of ≈580 nm per RIU and surface sensitivity of ≈1900 pm nm^{-1} in a standard bio-sandwich assay.[178,179] Very recently, the concept of "multi-box" waveguide has been further investigated with the incorporation of Bragg grating[180] and MZI-based[181] sensing structures.

4.2. Strategies for Simplifying the Biosensing Schemes

One key driving force behind the development of on-chip label-free optical biosensors is to minimize the demand for bulky and expensive instruments (e.g., high-precision wavelength-tunable lasers or off-chip spectrometers). In 2011, Claes et al. developed an on-chip wavelength interrogation scheme, which splits the transmission signals into multiple wavelength channels.[182] Adopting Vernier-cascade microrings as transducers and compact arrayed waveguide grating (AWG) for on-chip spectrum analysis, this scheme only requires a broadband light source and an IR camera for monitoring the output intensity signal in parallel. Later Song et al. reported a similar biosensing scheme working with a broadband light source,[183] as shown in **Figure 8**a. Here the optical resonance shift in the sensing ring is traced by electrical tuning of the reference ring. Therefore only a compact, cost-effective powermeter working in the IR wavelength is required. In 2018, Moock et al. reported a similar electrical tracing-based sensing concept for serially cascaded ring resonator arrays in the fashion of time-division multiplex.[184] Relying on a low-cost fixed wavelength laser source at the telecommunication band, the read-out rate can be improved from sub-Hz in conventional tunable laser-based schemes (limited by the scanning speed) to 100 Hz.[184] However, only refractive index sensing for droplets was testified whereas label-free biodetection has not been reported.

Nevertheless, the SOI material platform and telecommunication wavelength for biosensing are not the best choices for cost-effective biosensors because the camera or light source in IR wavelengths are still relatively expensive and not ubiquitous. Compared to silicon, SiN featuring a transparency window in shorter wavelengths (<1.1 μm) is highly sought for a miniaturized low-cost system utilizing widely available light sources such as LEDs, laser diodes and CMOS cameras. Recently,

Martens et al. developed a SiN MZI-based biosensing system working in the wavelength around 850 nm using a superluminescent diode,[94] which is compatible with the response range of CMOS cameras. As illustrated in Figure 8b, the signal is filtered by AWG into 30 channels so that the spectrum can be reconstructed from the discretized data by fitting. Hence the spectral shift of interferometer signal can be traced in real-time.

Since 2014, Wang et al. have been developing multi-element cascaded microrings, also termed "coupled-resonator optical-waveguide (CROW)" as a biosensor using elastic light scattering-based pattern recognition technique (see Figure 8c,d).[185] The calibrated sensing system only requires a fixed-wavelength laser diode and a CMOS camera.[186] In the latest demonstrations of streptavidin detection using surface-functionalized CROWs, the varying light scattering patterns are recorded and analyzed through a correlation algorithm so that the relative spectral shift can be readily extracted.[85,187] In this scheme, an on-chip spectrometer such as an AWG is circumvented, which largely minimizes the sensor footprint and facilitates multiplexed detection on a single chip. As presented in Figure 8e, the miniaturized optofluidic integrated CROW biosensor chip can work with a smartphone camera through a PDMS soft lens as the optical interface, which paves the way toward POC applications.

5. Laboratory Prototypes toward POC Applications

In recent years, various developed laboratory prototypes further approach the envisaged goal of miniaturized and multi-functional lab-on-a-chip optical bioanalytical systems.[188] Integrating a biosensor chip with advanced microfluidic processing units and optoelectronic components render the technology closer to commercialization. **Table 3** summarizes the state-of-the-art laboratory prototypes with integrated microfluidic modules or optoelectronic components.

5.1. Laboratory Prototypes with Advanced Microfluidic Integration

In 2017, Szydzik et al. reported a multiplexed BiMW-based biosensor chip integrated with pneumatic valve-based microfluidic modules offering a high degree of flexible, automatic and on-chip sequential manipulation of multiple fluidic samples.[192] As illustrated in **Figure 9**a,b, utilizing a one-step injection molding technique, a thin PDMS slab-based microfluidic channel was integrated with the silicon sensor chip and also a thick PDMS interface slab. An automatic competitive immunoassay was performed with "cycles" of reference and competitive assays for detecting tetracycline antibiotics.

Apart from developing sophisticated microfluidic circuits on top of the sensor chip, it is highly desirable to utilize low-cost polymer microfluidic cartridges made by injection molding with mass production where the chip-scale label-free optical biosensors serve as the inserted and replaceable element. Nowadays, cartridge-based microfluidics emerges as a promising technology for in vitro diagnostics.[195] Typical microfluidic cartridge integrates storage, handing of fluidic samples or reagents as well
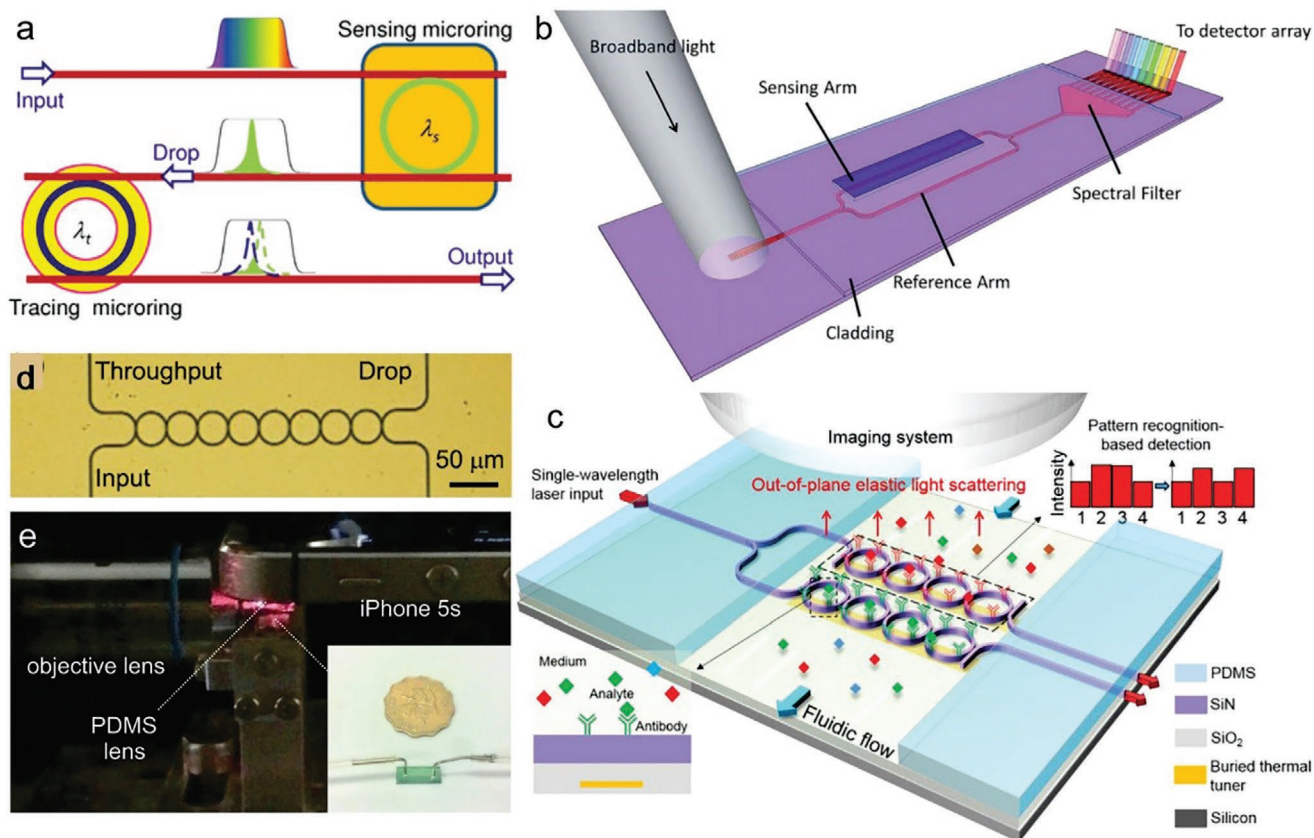
Figure 8. a) Schematic showing the working principle of electrical tracing-assisted dual-microring based biosensors working without the wavelength scanning step. Reproduced with permission.[183] Copyright 2012, The Optical Society. b) Schematic showing a SiN MZI-based biosensor integrated with an on-chip AWG spectral filter. Reproduced with permission.[94] Copyright 2018, Royal Society of Chemistry. c) Schematic of multiplexed SiN CROW-based biosensors working with a fixed-wavelength laser diode and a CMOS camera. d) Optical microscope image of an 8-element SiN CROW. Reproduced with permission.[85] Copyright 2018, IEEE. e) Experimental setup for measurement with a smartphone and PDMS miniaturized soft lens. Inset: Picture of an integrated CROW-based optofluidic sensor chip.

Table 3. Summary of laboratory prototypes for chip-scale silicon-based optical biosensors.

| Year	Material platform	Sensor configuration	Fluidic control	Multiplex capability	Major demonstrations	Ref.
2012	SOI chip integrated with electrowetting-on-dielectric substrate	Microring array	Digital microfluidic	Single droplet, 12 microrings at one site	Refractive index sensing	[189]
2015	Si₃N₄-on-silica chip integrated with PDMS channels	BB-MZI with integrated LEDs	Syringe pump	Single channel with 10 transducers	Protein binding reaction	[190]
2016	SiN-on-silica chip integrated with PDMS microfluidic cartridge	Microring array	Controlled by electrolysis cell	2 assays performed on a chip, sensing chamber with 14 sensors	Automatically performed immunoassay	[191]
2017	SiN-on-silica chip integrated with PDMS microfluidic channels	BiMW array	Pneumatic valve	2 channels	Automation of cyclic competitive immunoassays	[192]
2018	SiN-on-silica chip integrated with PDMS microfluidic cartridge	MZI and AWG filters	Syringe pump with a flow monitoring system	Single channel with 6 pairs of sensors	Detect biomarker of tuberculosis in clinical samples	[94]
2018	SOI chip with fan-out wafer-level-packaging process	Microring array and on-chip Ge PDs	Syringe pump	2 channels, each with 8 sensing areas	Bioassay of detecting streptavidin	[193]
2019	Si₃N₄-on-silica chip integrated with PDMS channels	BB-MZI and AWG filters, with on-chip integrated LED and PD arrays	Controlled with a fluidic cartridge	Single channel with 10 transducers	Real-time binding detection and the immunochemical CRP detection	[194]
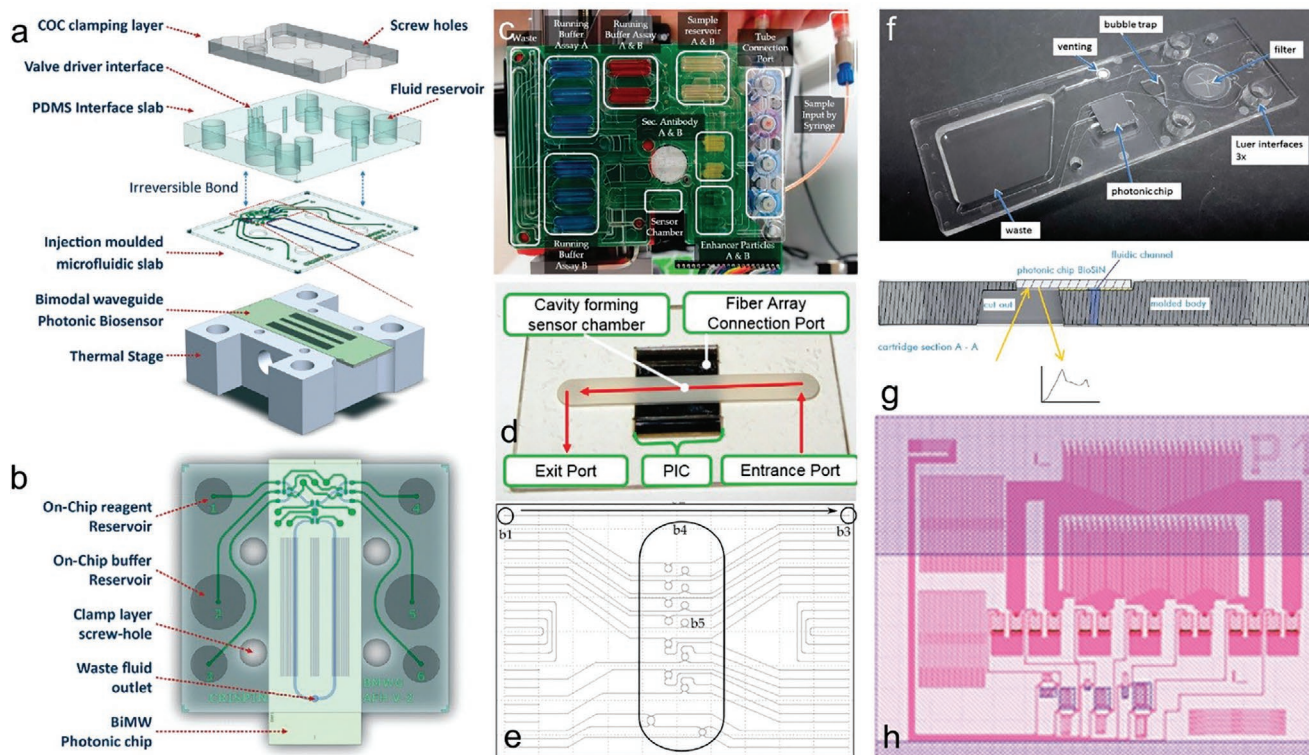
Figure 9. a) Schematic of an automated microfluidic module integrated with a BiMW biosensor chip mounted on a thermal stage. b) Top-view schematic showing primary fluidic reservoirs and microfluidic channels aligned with optical biosensors. Reproduced with permission.[192] Copyright 2017, Royal Society of Chemistry. c) Picture of a microfluidic cartridge on a PCB for activating the electrolysis cells. The reservoirs are filled with colored waters. d) Picture showing the flow cell on top of a sensor chip. Sensor chips (not shown here) can be inserted at the sensing chamber. e) The layout design of microring-based sensor array. Regions "b1" and "b3" denote grating couplers for coupling in and out of laser light. Reproduced with permission.[191] Copyright 2016, the MDPI. f) Picture of a microfluidic cartridge. g) Schematic cross-sectional view of the cartridge integrated with a sensor chip. h) Layout of photonic circuits with MZI (in the middle) and AWG arrays (upper shaded region). Reproduced with permission.[94] Copyright 2018, Royal Society of Chemistry.

as waste chambers into a single, compact, and disposable unit, which largely facilitates automated sample delivery for sensing process and also minimizes the required sample volume.

In 2016, Geidel et al. reported a SiN microring-based biosensor chip integrated with a self-contained microfluidic cartridge.[191] The integrated active micropump operated through gas generated by electrolytic cells largely streamlines the sensing process with a minor requirement of external electronic infrastructure. Figure 9c shows the cartridge layout for running two immunoassays. As presented in Figure 9d, only the central region of the sensing chamber is exposed and interacted with the delivered fluidic flow (see Figure 9e). Light gets coupled in and out using fiber arrays and on-chip grating couplers on two sides. The automatically performed in situ immunoassay was demonstrated with selective capture of GroEL proteins and surface-coated nanoparticles for signal enhancement.

In 2018, Martens et al. developed a low-cost SiN MZI-based biosensing chip integrated with a polymer microfluidic cartridge providing an automatic fluidic handling process, as shown in Figure 9f,g.[94] Figure 9h displays the sensor layout with six multiplexed BB-MZI biosensors with corresponding AWGs working in the wavelength of ≈900 nm. Only off-chip LEDs and a camera are required without the need to process critical optical alignments, which renders the system affordable for

POC applications.[94] Immunoassays were carried out with label-free detection of CRP with a calibrated LOD of 19.5 ng mL^{-1}. Recently, the system has also been successfully applied for tuberculosis diagnosis using clinical urine samples from patients.[97]

Digital microfluidics technology appears in recent years as a promising route for lab-on-a-chip systems via handling microdroplets instead of continuous flows in common microfluidic systems.[196,197] As the most common working principle, electrowetting describes a change of interfacial tension due to the applied electric field between the liquid and dielectric surface and allows transport of microdroplets to the sensing area. The latest technology features a minimized sample volume and pump-free liquid delivery in which various potential issues (e.g., channel clogging, air bubble formation, sample cross-contamination) can be avoided. In 2012, silicon microring-based sensors were incorporated into a digital microfluidic system with high throughput and compact footprint.[189] In **Figure 10**a, typical digital microfluidic chips contain an indium tin oxide (ITO)-covered glass top plate. Here, the sensor chip is applied as the top plate for integrating with the digital microfluidic system with embedded electrodes (see Figure 10b,c). Cascaded microring sensors are probed by a wavelength-tunable laser and the spectral signals are read out by an IR camera (see Figure 10d). Bulk refractive index sensing experiment was performed with free controlling the
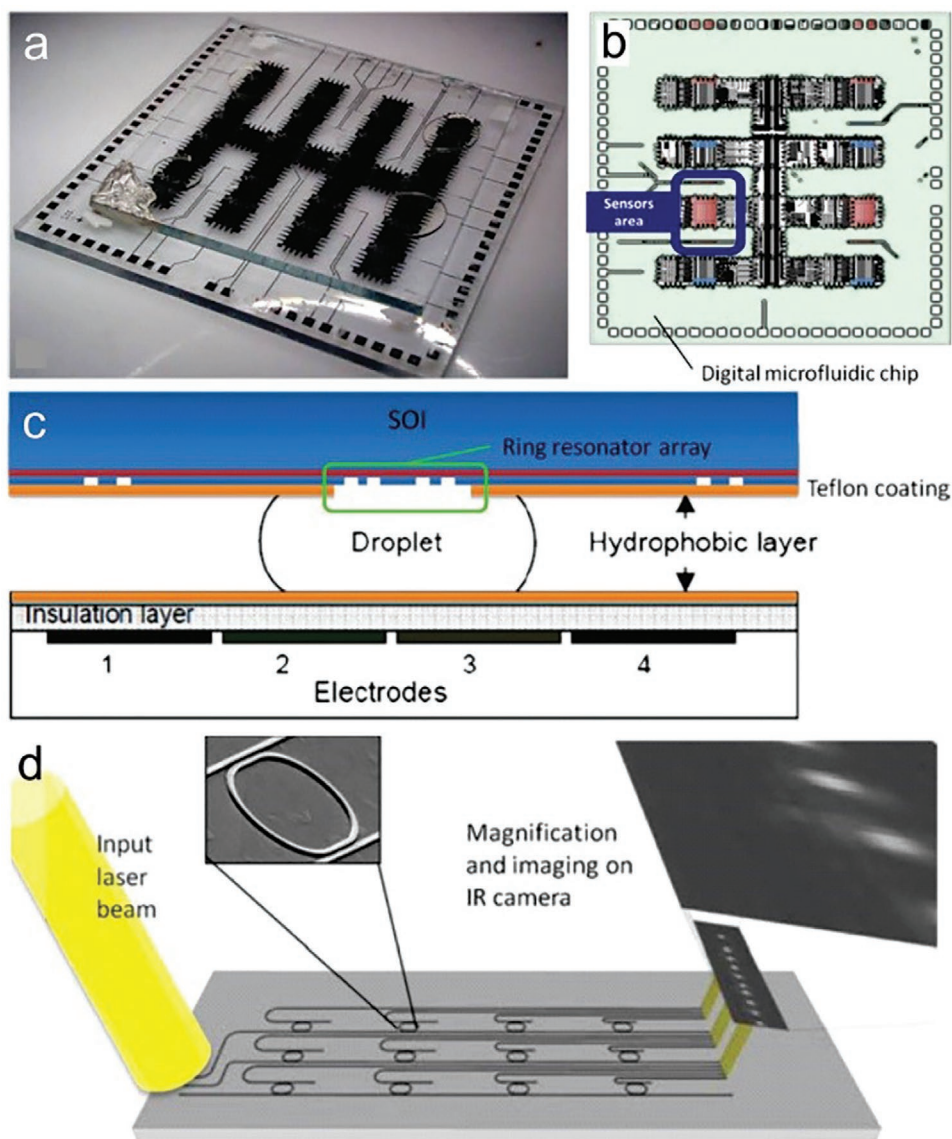
**ADVANCED
SCIENCE NEWS**
www.advancedsciencenews.com

**ADVANCED
MATERIALS
TECHNOLOGIES**
www.advmattechnol.de

Figure 10. a) Picture of a digital microfluidic chip covered with a standard ITO top plate on top with droplets in between. b) Design layout showing the alignment between a digital microfluidic chip and SOI sensor chips. c) Schematic cross-sectional view of a digital microfluidic system incorporated with a SOI-based sensor chip. d) Schematic showing the design of PICs with 12 multiplexed microrings. Reproduced with permission.[189] Copyright 2012, Springer Nature.

droplet of sodium chloride solutions. However, surface functionalization of transducers for biosensing has not been reported. In 2017, Wondimu et al. developed WGM optical microcavity-based label-free biosensing incorporated in a digital microfluidic system with demonstrated streptavidin detection.[198] However, the cavities are not silicon-based but made of polymethyl methacrylate (PMMA), which require bulky instruments (i.e., a high-power pump laser and spectrometer) and optical focusing with free-space optical components for measurements.

5.2. Laboratory Prototypes with On-Chip Optoelectronic Devices

One major obstacle of commercializing silicon-based integrated optical biosensing techniques into low-cost, disposable POC systems is the demand for off-chip optoelectronic equipment such as external light source, spectrometer, PD/camera, and also necessary parts for light coupling (e.g., lenses or fiber array). Monolithic integration of both passive optical sensors and active optoelectronic devices on a single sensor chip is hence highly sought after.[199–201]

In 2018, Laplatine et al. reported silicon microring-based biosensors integrated with on-chip germanium PDs using fan-out wafer-level-packaging.[193] Sixteen independent microring resonators and associated germanium PDs were fabricated on a 1 mm² die (see **Figure 11**a) and packaged onto a chip with electrical interconnects and SU8 microfluidic channels, as presented in Figure 11b. The sensor chip after packaging is integrated with spring-loaded pins and also a PMMA/PDMS-based fluidic gasket (see Figure 11c,d). For such a
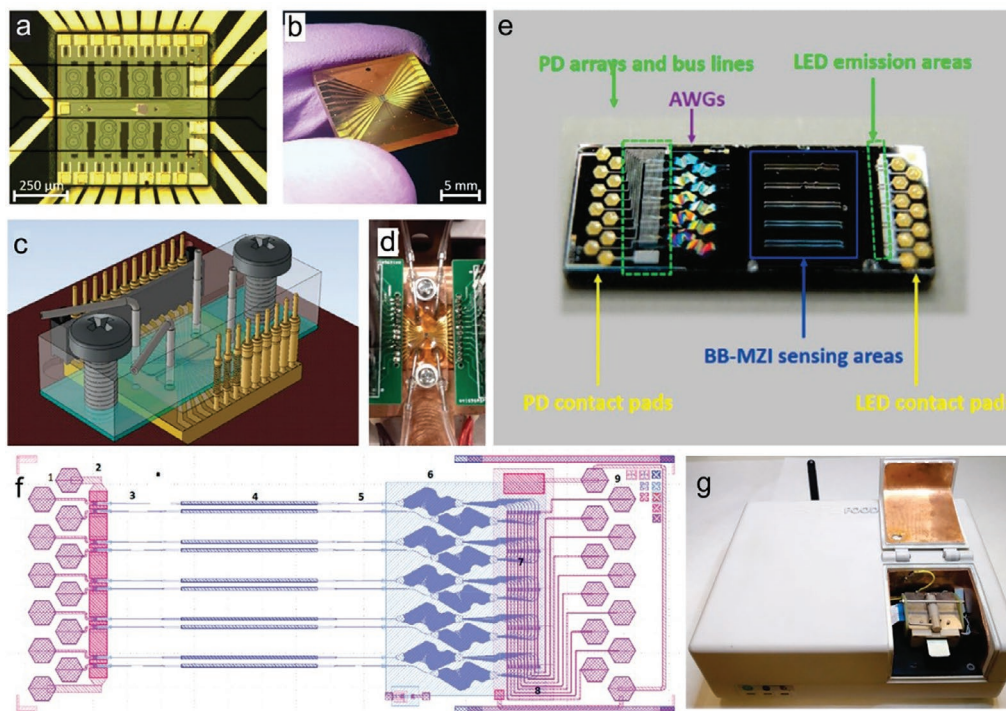
**ADVANCED
SCIENCE NEWS**

www.advancedsciencenews.com

**ADVANCED
MATERIALS
TECHNOLOGIES**

www.advmattechnol.de

Figure 11. a) Optical microscope image of a fabricated sensor die with 16 microring arrays and 16 PD arrays for multiplexed detection. b) Picture of the integrated sensor chip. c) Schematic of the fabricated optofluidic chip with PDMS channel cover and spring-loaded pins. d) Picture of the prototype showing the connection with PCBs on a base controlled with a thermoelectric cooling module. Reproduced with permission.[193] Copyright 2018, Elsevier. e) Picture of the sensor chip with integrated MZIs, AWGs, LEDs, and PDs. For LEDs and PDs, only contact pads can be discernible here. f) Layout of the optoelectronic biosensor chip. The numbers denote: 1) LED contact pads; 2) LED junctions; 3) on-chip mode converters; 4) BB-MZI sensing region; 5) on-chip mode converters; 6) on-chip AWG-based spectral analyzers; 7) PD array; 8) PD bus lines; 9) PD pads. g) Picture of the portable reader with dimensions of $20 \times 16 \times 7$ cm^3. Reproduced with permission.[194] Copyright 2019, American Chemical Society.

prototype, the pins are connected with standard header pins via a printed circuit board (PCB). Both bulk refractive index sensing and label-free bioassay of streptavidin detection were performed.

Misiakos et al. developed SiN BB-MZI array-based label-free biosensors with monolithically integrated avalanche-type LEDs as on-chip waveguide-coupled light sources.[190,202] The on-chip integrated avalanche diodes working in the reverse-biased mode emit with a wide band from visible to near-IR. However, an off-chip spectrometer is still required. Notably, in 2019, the same group further developed a "fully spectroscopic" chip-scale label-free biosensor with monolithically integrated light sources and PDs.[194] As shown in Figure 11e,f, ten multiplexed BB-MZI transducers are coupled with their own on-chip broadband light sources. After filtering with AWGs, the light beams are out-coupled to on-chip integrated PD arrays for analyzing the output spectra. Moreover, such a portable reader compromising a docking station for accommodating the "opto-electro-fluidic" biosensor chip, a micropump, driver and read-out circuits for LEDs and PDs, microcontrollers and communication electronics was also established (see Figure 11g). Real-time monitoring of the binding reaction for mouse IgG was presented with the lowest distinguishable concentration of 60 pM. Direct determination and detection of CRP in human serum

were also performed with the lowest detectable concentration of 20 ng mL^{-1}.

6. Current Commercial Chip-Scale Evanescent Field-Based Biosensors

In the past two decades, the continuous advances of integrated photonics and label-free optical biosensing technologies give rise to successful technology transfer from research laboratories to businesses. Various optical biosensing systems based on dielectric on-chip photonic devices become commercially available. **Table 4** summarizes the relevant optical label-free biosensing systems currently on the market. Most of them feature on-chip optical waveguides or grating structures as sensors integrated with microplates or microfluidic channels on a glass substrate. However, bulky components are still unavoidable, such as external light source, fluidic pump, data storage, and processing units, etc.

In 2005, "EPIC" was announced by Corning as the first benchtop optical system for label-free biochemical sensing and cell-based assays. The plate-based sensor chip consists of waveguide resonant gratings.[203] A broadband light source is employed for probing the resonances and the reflected light is measured by a spectrometer (replaced by a camera in the latest

ADVANCED
SCIENCE NEWS
www.advancedsciencenews.com

ADVANCED
MATERIALS
TECHNOLOGIES
www.advmattechnol.de

Table 4. List of currently commercialized label-free biosensing systems on the market based on dielectric photonic chips.

Instrument (Company)	Material platform	Core technology	Fluidic condition	Multiplex capability	Main functionalities
EPIC system (Corning)	Glass	Resonant waveguide gratings	Plate-based	384 well plate	Detection of enzyme, small molecule, protein and DNA; antibody and cell-based studies
ResoSens system (ResonantSensors)	TiO_2	Resonant waveguide gratings	Plate-based	96 or 384 well plate	Cell-based assays and antibody–antigen interactions
OWLS system (Microvacuum)	$Si_xTi_{(1-x)}O_2$ on glass	Optical waveguide and grating couplers	Flow [0.1 µL min^{-1} –30 mL min^{-1}]	Single measurement	Protein adsorption; antigen antibody binding; drug screening, binding kinetics; immunosensing
Creoptix WAVE system (Creoptix AG)	Ta_2O_5 on glass	Grating-coupled interferometry	Flow [up to 400 µL min^{-1}]	2 or 4 channels	Small-molecule characterization; kinetic analysis; drug test
Maverick system (Genalyte)	SOI	Microring arrays	Flow [up to 30 µL min^{-1}]	2 channels, 16 analytes per channel	Protein binding events, mass concentration detection, etc.

models). Likewise, the "ResoSens" system developed by Resonant Sensors makes use of a similar grating structure based on TiO_2 substrate for label-free bioassays. Afterward, a biosensing system featuring "optical waveguide lightmode spectroscopy (OWLS)" technique was developed by Microvacuum. The sensor structure combines a grating coupler and optical waveguide.[204] A linearly polarized red laser light is coupled into the grating coupler with an optimized incidence angle and then guided by TIR to the output port where it is detected by a PD. The whole system is integrated on a precision goniometer so that any perturbation on the sensor surface can be extracted by monitoring the variation of incidence angle.

In 2014, "Creoptix WAVE" was launched as a new label-free test bench with 4-channel real-time measurements. The grating-coupled interferometry (GCI) technique involves optical waveguides with two input coupling and one output coupling gratings, suggesting clear advantages compared to the traditional grating coupler-based biosensors.[205,206] Owing to the waveguide-based interferometry, the analyte information is extracted through a time-dependent and robust phase shift signal. Thus the noise from temperature shifts or mechanical distortions can be largely mitigated compared to the traditional scheme of detecting interference signals at the far-field. While the product is based on the Ta_2O_5-on-glass material platform, researchers have also demonstrated the GCI technique on the silicon platform in research laboratories.[207]

Genalyte has been developing the "Maverick" detection system based on the latest silicon photonics technology over the past decade. The disposable and consumable sensing chip contains two fluidic channels and each channel covers 16 waveguide-coupled microring-based sensing units.[208] Single test against 16 analytes can be performed with a low sample consumption down to 5–10 µL in only 10 min. In particular, the system performs biomolecule assays in multiple complex matrices such as serum, plasma, whole blood, and crude extracts, which largely simplifies the sample preparation step. Besides, quantitative mass concentration detection has been reported for industrial polymer using the Maverick system.[209] The extracted "polydispersity index" is in a good agreement with standard methods (e.g., differential refractive index detectors and UV chromatogram). Very recently, the system has been employed on clinically diagnosed patients for 12 assays of simultaneously detecting autoantibodies in whole blood within less than 15 min, suggesting clear advantages over standard clinical tests.[210]

7. The Roadmap for Future Silicon-Based Optical Biosensors

Figure 12 presents an overview of technology developments on on-chip integrated dielectric photonic devices for label-free biosensing. Basic building blocks in silicon photonics, such as slab waveguides, straight ridge waveguides, multimode waveguides, and resonant gratings were exploited for optical biosensing at early stages. Then functional photonic devices originally for on-chip optical signal processing in communications and interconnects such as microrings and interferometers were also employed for biosensing. Many of these techniques have been successfully commercialized as bioanalytical systems on the market while others are under tests with clinical samples of patients for in vitro medical diagnostics. In the past decade, advanced sensor designs and alternative sensing mechanisms appear, such as those with multiple cross-coupled units (e.g., cascaded rings with Vernier effect, CROWs), or fine engineered sub-wavelength structures for either light localization (e.g., PhCs, metasurfaces) or lossless propagation with a large mode overlapping to the analytes (e.g., SWG structure). These relatively new techniques are still attracting extensive research investigations from research groups over the world. Regarding the future development, various new findings and fresh concepts in optical physics may point the way for next-generation silicon-based on-chip biosensors to unprecedented sensing performance in terms of sensitivity, LOD, time resolution, specificity, stability, etc.

7.1. Toward Ultra-Sensitive Biodetection Systems

Detecting single biological entities is always a crucial topic in fundamental science.[25,28] Although plenty of strategies have been explored toward ultra-sensitive detection, the typical LOD of current silicon-based planar optical biosensors are mostly ~ fM to nM. To our knowledge, single-molecule detection
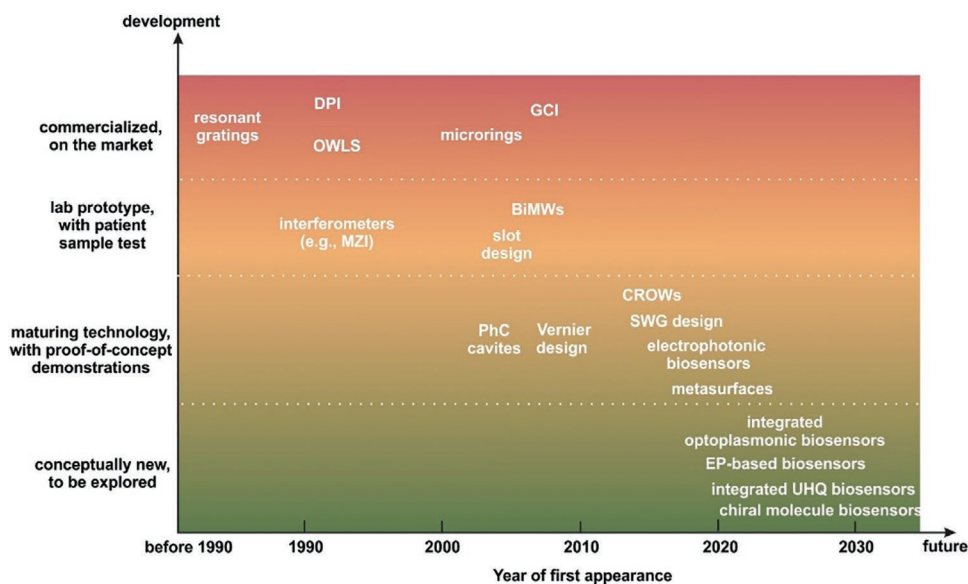
**ADVANCED
SCIENCE NEWS**
www.advancedsciencenews.com

**ADVANCED
MATERIALS
TECHNOLOGIES**
www.advmattechnol.de

Figure 12. The past, state-of-the-art and our envisioned future development of dielectric chip-scale integrated label-free optical biosensing techniques.

has not been reported yet. Remarkably, in recent years, probing single molecules has been accomplished using ultra-high-Q (UHQ) dielectric WGM microcavities such as microspheres and microtoroids.[28,211–215] **Figure 13**a schematically presents the biosensing system using a microsphere-based UHQ cavity. However, these pillar-supported WGM microcavities have some inherent drawbacks. First, the involved sophisticated fabrication process (e.g., wet etching and thermal reflow) inhibits the mass production. Second, the freestanding UHQ cavities require a highly critical light coupling condition (e.g., using a tapered fiber or bulky prism). At last, it is technically challenging to incorporate into complex photonic and microfluidic circuits for automatic and multiplexed measurements. For most of the on-chip microring or PhC-based biosensors, the moderate Q factor $\approx 10^2$ to 10^4 hinders the optimization of LOD compared to those of standalone UHQ WGM microcavities ($Q \approx 10^7$–10^9).[216]

In recent years, Bowers and Lipson's research groups are leading the research on on-chip integrated UHQ WGM microresonators based on ultra-low loss Si_3N_4 for enhanced optical nonlinear effects.[217,218] Figure 13b shows a fabricated waveguide-integrated UHQ microring. The measured transmission spectrum in Figure 13c suggests a well-resolved backscattering-induced mode splitting feature. Loaded Q factors up to $\approx 7 \times 10^7$ for integrated microrings have been realized by fine-tuning the material composition in Si_3N_4 to minimize the absorption loss and developing new surface smooth techniques (e.g., chemical mechanical polishing of deposited Si_3N_4 films, multipass lithography, and hard mask-based dry etching) to minimize the scattering loss.[217] In 2018, Yang et al. reported a monolithically integrated UHQ silica WGM ridge resonator coupled to a SiN waveguide with a measured $Q \approx 10^8$ (see Figure 13d).[219] Figure 13e displayed the mode profile around the resonator-waveguide coupling region. These waveguide-coupled UHQ microcavities can be further developed into an optofluidic integrated ultra-sensitive biosensor, which will promise a leap forward on label-free detection down to single-molecule regimes in the near future. Notably, UHQ WGM microcavities working at

an exceptional point (EP) as the degeneracy of two or multiple eigenstates reveal a much-enhanced sensitivity toward localized nanoparticle-induced perturbations.[220] The induced mode splitting around the second-order EP suggests a square-root dependence of the perturbation rather than the linear dependence in conventional cavities. Same concept of EP-enhanced sensing can be extended using silicon-based on-chip photonic devices for ultra-sensitive biodetection.

The concept of combining on-chip optical and plasmonic sensors shed light on ultra-sensitive detections. Chatzianagnostou et al. developed an integrated optical sensor consisting of a silicon nitride MZI and a gold stripe as a plasmonic waveguide with a butt-coupled interface (see Figure 13f).[221] Besides, active thermal tuning elements including a variable optical attenuator (VOA) and a phase shifter were deployed for spectrally tuning to the desired spectral window with a maximized extinction ratio and optimizing the LOD. Proof-of-concept refractive index sensing experiments in Figure 13g suggest a bulk sensitivity up to 1930 nm per RIU. However, biomolecule detection based on such a hybrid sensor has not been reported.

Apart from realizing mode conversion between independent photonic and plasmonic elements, new hybrid "optoplasmonic" modes have been explored by integrating metal nanostructure with photonic devices. Remarkably, the optoplasmonic WGM microcavities simultaneously benefit from ultra-small modal volumes,[222,223] high Q-factors, and extreme near-field enhancements (also termed "plasmonic hotspot"). Furthermore, for on-resonance states, the enhanced local electric field intensity due to oscillation of free electrons in metals at the sensing site leads to a boosted sensitivity to tiny perturbations.[28,224,225] In 2016, Kim et al. reported real-time in situ monitoring of both transient and permanent ligand surface interactions using a silica UHQ microsphere with immobilized gold nanorods. The chemical reaction between the head groups of single ligand molecules and gold atoms can be analyzed and categorized into two regimes, namely with high and low affinities (see Figure 13h). Through tracing the resonance shift in real-time in
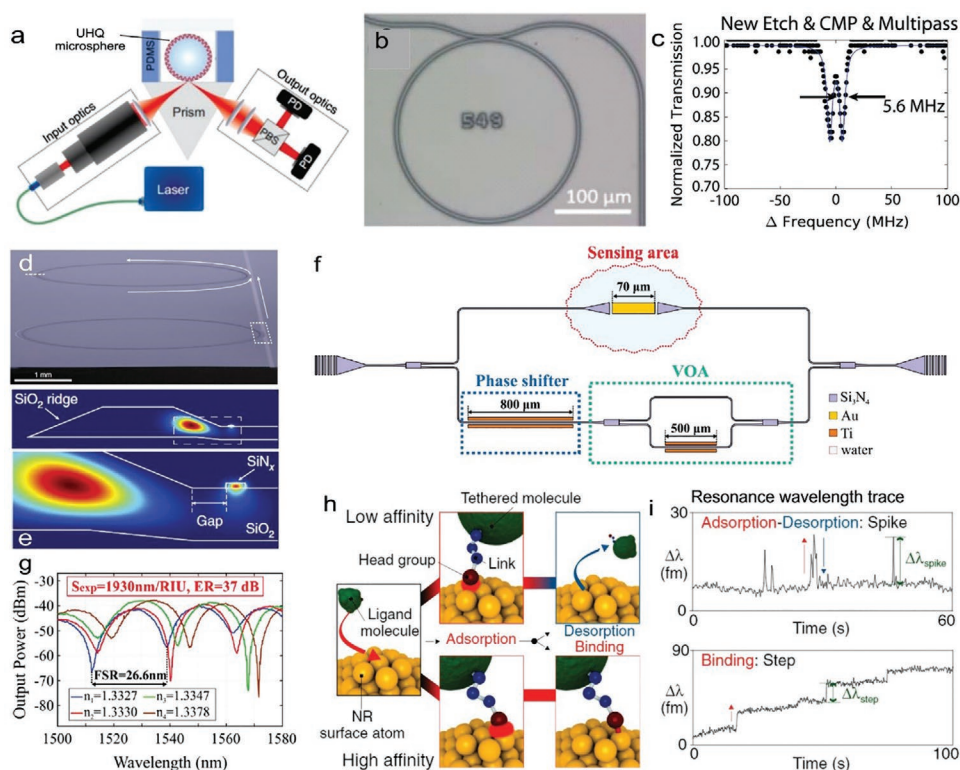
Figure 13. a) Schematic showing the WGM microsphere-based biosensing system. Reproduced with permission.[224] Copyright 2018, De Gruyter. b) Optical microscope image of a waveguide-coupled UHQ microring with an optimized fabrication process. c) Normalized transmission spectrum of a UHQ microring. Reproduced with permission.[217] Copyright 2017, The Optical Society. d) SEM image of two ridge resonators coupled with a common waveguide. e) Simulated mode profile at the ridge resonator-waveguide coupling region in a cross-sectional view. Reproduced with permission.[219] Copyright 2018, Springer Nature. f) Schematic of the plasmo-photonic MZI sensor with a gold strip-based plasmonic waveguide as the sensing element. g) Measured spectra in refractive index sensing of still water and PBS solutions. Reproduced with permission.[221] Copyright 2019, American Chemical Society. h) Sketch of the two types of reactions between ligand and metal nanorod decorated on a microsphere. i) Trace of resonance shift for two types of reaction. Upper: the low-affinity regime showing transient interactions. Lower: the high-affinity regime showing covalent bindings. Reproduced with permission.[233] Copyright 2016, Wiley-VCH.

Figure 13i, a transient reaction causes a spike pattern whereas a covalent binding generates a step pattern. More recently, monitoring the conformational dynamics of single protein molecules has been achieved by optoplasmonic UHQ WGM sensors.[226]

Over the past few years, integrating plasmonic nanostructures into silicon-based micro/nanophotonic devices have been continuously explored on a wide range of applications for nanolasers,[227] on-chip optical manipulation,[228] and SERS.[229] However, to our knowledge, integrating plasmonic nanostructure with silicon-based on-chip devices for biodetection has been discussed only in theoretical studies.[230–232] We envision that on-chip integrated hybrid optoplasmonic optical biosensors will bring about unprecedented sensing performance in the coming years.

7.2. Toward Multi-Functional Biodetection Systems

Apart from ultra-sensitive biodetection, it is of great significance to empower the sensing functionalities on the same platform with other alternative optical and non-optical sensing principles. The latest discoveries in fundamental optical physics may inspire the development of new biosensing mechanisms. As an example, on-chip generation of chiral light in exotic waveguiding structures[234,235] could be applied for discrimination and quantification of chiral molecules. Furthermore, compared to evanescent field-based detection, electrical or magnetic detection can offer additional information on various bioactivities, such as monitoring the electrochemical activities at the transducer surface and detecting analytes that are far away from the transducer surface. The realization of electro-photonic microring-based biosensors is the first step of combining on-chip optical and electrical sensors.[134] In the future, we expect a burgeoning field of integrated silicon-based biosensors working with different principles.

In recent years, nanomembrane-based rolled-up microtubes have been successfully integrated with silicon-based waveguides,[236,237] and later demonstrated as vertical WGM optical microcavities for optofluidic sensing.[238] **Figure 14**a schematically presents self-rolled vertical microtubes monolithically integrated on silicon waveguide arrays. The ultra-thin cavity wall (≈100–200 nm) ensures strong evanescent fields and thus efficient interactions between the WGMs and the objects inside the hollow core as the sensing channel.[239] Compared to other freestanding tubular-shaped optical biosensors[240] (e.g., microcapillaries[54] and microbubbles[241]), rolled-up microtubes feature a highly flexible integration with on-chip optical,
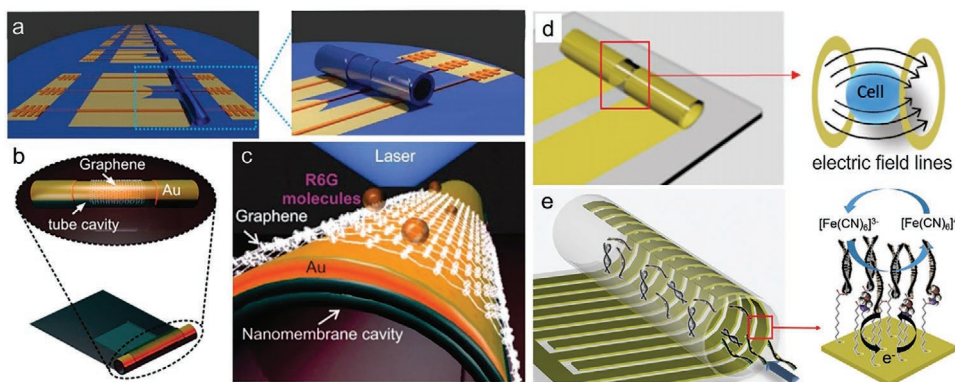
Figure 14. a) Schematic showing vertical rolled-up microcavities integrated with waveguide array on an SOI chip. Reproduced with permission.[236] Copyright 2015, The Optical Society. b) Schematic of a graphene-activated optoplasmonic rolled-up microcavity-based biochemical sensor. c) Schematic showing the zoomed-in view at the tube sensor surface for monitoring the photodegradation of dye molecules. Reproduced with permission.[245] Copyright 2019, American Chemical Society. d) Schematic of conductometric tubular electrodes for single-cell in-flow detection. e) Schematic of interdigital electrodes for monitoring electrochemical reactions. In particular, the coverage of the electrode surface by the hybridized DNA can be determined by the reduction/oxidation of ferricyanide and an anionic solution. Reproduced with permission.[240] Copyright 2019, American Chemical Society.

electrical, magnetic devices, and microfluidic circuits,[242] and hence can be utilized as a central building block for lab-on-a-chip biosensing systems.

Thanks to the maturing rolled-up nanotechnology, various nanomembrane-based tubular sensors working in different principles have been developed in the past few years,[240] including silica-based microtubes as optical[243,244] or optoplasmonic[245] cavities for probing the binding dynamics of molecules. In 2019, graphene-integrated optoplasmonic microtubes have been employed for sensitive surface detection due to the largely enhanced electric field (see Figure 14b,c).[245] Monitoring the photodegradation process of dye molecules with resolution down to the single molecular layer was achieved. Besides, leveraging this versatile nanotechnology, tubular electrodes have been developed as electric biosensors for real-time cell-based assays[246] (see Figure 14d) by conductometric measurements and also detecting hybridization of complementary DNA strands[247] by impedimetric measurements (see Figure 14e). In the future, all these fascinating biosensing architectures can be merged and integrated onto a silicon chip as a multi-functional opto-electro-fluidic bioanalytical system.

7.3. Toward Portable Systems for Smartphone-Based Routine Diagnostics

Over the past two decades, the concept of "mobile health" has been continuously explored, which aims at implementing the practice of medicine and healthcare via mobile devices and wireless technologies.[248–250] The latest models of smartphones incorporate powerful computing capabilities, large data storage, network connectivity, and a large variety of sensors/detectors such as CMOS cameras, touch screens, sound detectors, gyroscopes, etc. Nowadays, the demonstrated smartphone-based diagnostics include optical microscopy (e.g., brightfield, fluorescence, scattering),[251] spectroscopy,[252] colorimetric detection,[253] and electrochemical detections.[254] Well-established tests originally performed with bulky instruments including label-free immunoassays, cellular imaging, lateral flow assays have been accomplished using such a miniaturized smartphone-incorporated system.[250] For label-free bioassays, chip-scale SPR structures [255,256] and dielectric gratings (also termed 1D PhCs)[257–259] have been successfully integrated with smartphones as portable biosensors. However, free-space optical components (e.g., lens, filters, prism) and an external light source (LED, or laser diode) cannot be circumvented, which renders the system relatively bulky and less convenient.

To our knowledge, reports on integrating silicon-based chip-scale biosensors with smartphones are still scarce. Now it is the right moment to drive for smartphone-based miniaturized systems leveraging the latest silicon-based label-free biosensing technologies for routine POC tests. An ideal plan may incorporate the following units: i) a silicon sensor chip with multiplexed passive optical transducers selectively functionalized with different receptors for corresponding biomarkers and reference units fabricated at the wafer level which can be freely replaced; ii) a reusable microfluidic circuit including miniaturized valve and pump with sample handling capabilities, or a recently reported "plug-n-play" module with digital microfluidics;[260] iii) a dock offering proper alignment between the passive sensor chip and off-chip optoelectronic components (light source and camera) in the smartphone for light coupling; iv) an electrical interface between the optofluidic chip and smartphone for maneuvering the automatic bioassays; v) software for real-time processing the sensing results, and sharing results via the cloud. Without introducing on-chip active optoelectronic devices (e.g., light sources or PDs), the silicon sensor chip can be made with very low cost and hence disposable after use, which also avoids complex cleaning and potential cross-contamination issues. Although the technology is still in early infancy compared to other portable optical bioanalytical devices running conventional tests like ELISA and real-time polymerase chain reaction for POC assays,[261] we expect a technology boom for integrating and coordinating these label-free biosensing techniques with smartphones in the coming 10 years.

**ADVANCED
SCIENCE NEWS**
www.advancedsciencenews.com

**ADVANCED
MATERIALS
TECHNOLOGIES**
www.advmattechnol.de

8. Conclusion

In the burgeoning research area of chip-scale miniaturized biosensors, silicon-based photonic devices offering the promising platform with unprecedented opportunities are increasingly attracting research attention. The key and unique advantages mainly include: i) the CMOS compatible fabrication process; ii) the maturing silicon photonics technology with a plethora of device configurations as integrable sensing units; iii) the straightforward optofluidic integration routes; and iv) the well-established surface functionalization strategies. In this article, we have reviewed on the state-of-the-art and future development trend of silicon-based label-free optical biosensors utilizing on-chip lightwave guiding and evanescent field-based sensing principle. Cutting-edge technological advances on three types of on-chip optical biosensor architectures, namely interferometers, microring resonators, and photonic-crystal-based cavities are summarized. The emerging strategies of elevating sensitivities and simplifying sensing schemes are also discussed. Besides, seminal progress on packaged laboratory prototypes with incorporated advanced microfluidic or optoelectronic components takes the field one significant step closer to real-world applications. To replace the bulky models in currently time-consuming standard clinical tests and offer better biosensing performance using silicon-based label-free lab-on-a-chip bioanalytical systems will be a vigorously pursued goal. Meanwhile, it is also highly intriguing to turn the biosensor chips into low-cost, user-friendly, portable, and disposable products taking the advantages of ubiquitous and powerful smartphones to perform multiple routine bioassays for future POC diagnostics. We envision this rapidly advancing field will make a revolutionary impact on the medical diagnostic and personal healthcare in the near future.

Conflict of Interest

The authors declare no conflict of interest.

[1] C. D. Chin, V. Linder, S. K. Sia, *Lab Chip* **2012**, *12*, 2118.
[2] S. Nayak, N. R. Blumenfeld, T. Laksanasopin, S. K. Sia, *Anal. Chem.* **2017**, *89*, 102.
[3] S. M. Yoo, S. Y. Lee, *Trends Biotechnol.*. **2016**, *34*, 7.
[4] C. S. Wood, M. R. Thomas, J. Budd, T. P. Mashamba-Thompson, K. Herbst, D. Pillay, R. W. Peeling, A. M. Johnson, R. A. McKendry, M. M. Stevens, *Nature* **2019**, *566*, 467.
[5] R. M. Lequin, *Clin. Chem.* **2005**, *51*, 2415.
[6] D. J. O'Shannessy, M. Brigham-Burke, K. Peck, *Anal. Biochem.* **1992**, *205*, 132.
[7] J.-F. Masson, *ACS Sens.* **2017**, *2*, 16.
[8] G. Zanchetta, R. Lanfranco, F. Giavazzi, T. Bellini, M. Buscaglia, *Nanophotonics* **2017**, *6*, 627.
[9] X. Fan, I. M. White, S. I. Shopova, H. Zhu, J. D. Suter, Y. Sun, *Anal. Chim. Acta* **2008**, *620*, 8.
[10] S. E. McBirney, D. Chen, A. Scholtz, H. Ameri, A. M. Armani, *ACS Sens.* **2018**, *3*, 1264.
[11] Y. C. Chen, X. Fan, *Adv. Opt. Mater.* **2019**, *7*, 1900377.
[12] D. Rodrigo, O. Limaj, D. Janner, D. Etezadi, F. J. G. De Abajo, V. Pruneri, H. Altug, *Science* **2015**, *349*, 165.
[13] M. Maisonneuve, I.-H. Song, S. Patskovsky, M. Meunier, *Opt. Express* **2011**, *19*, 7410.
[14] A. Krasnok, M. Caldarola, N. Bonod, A. Alú, *Adv. Opt. Mater.* **2018**, *6*, 1701094.
[15] J.-P. Renaud, C.-w. Chung, U. H. Danielson, U. Egner, M. Hennig, R. E. Hubbard, H. Nar, *Nat. Rev. Drug Discovery* **2016**, *15*, 679.
[16] T. McGrath, C. Elliott, T. Fodey, *Anal. Bioanal. Chem.* **2012**, *403*, 75.
[17] T. Chalyan, C. Potrich, E. Schreuder, F. Falke, L. Pasquardini, C. Pederzolli, R. Heideman, L. Pavesi, *Toxins* **2019**, *11*, 409.
[18] B. Chocarro-Ruiz, A. Fernández-Gavela, S. Herranz, L. M. Lechuga, *Curr. Opin. Biotechnol.* **2017**, *45*, 175.
[19] H. N. Daghestani, B. W. Day, *Sensors* **2010**, *10*, 9630.
[20] V. C. Özalp, *Anal. Bioanal. Chem.* **2012**, *402*, 799.
[21] S. Rau, G. Gauglitz, *Anal. Bioanal. Chem.* **2012**, *402*, 529.
[22] D. A. Markov, K. Swinney, D. J. Bornhop, *J. Am. Chem. Soc.* **2004**, *126*, 16659.
[23] K. Kneipp, Y. Wang, H. Kneipp, L. T. Perelman, I. Itzkan, R. R. Dasari, M. S. Feld, *Phys. Rev. Lett.* **1997**, *78*, 1667.
[24] N. P. Pieczonka, R. F. Aroca, *Chem. Soc. Rev.* **2008**, *37*, 946.
[25] A. B. Taylor, P. Zijlstra, *ACS Sens.* **2017**, *2*, 1103.
[26] J. D. Spitzberg, A. Zrehen, X. F. van Kooten, A. Meller, *Adv. Mater.* **2019**, *31*, 1900422.
[27] A. M. Armani, R. P. Kulkarni, S. E. Fraser, R. C. Flagan, K. J. Vahala, *Science* **2007**, *317*, 783.
[28] S. Subramanian, H. Y. Wu, T. Constant, J. Xavier, F. Vollmer, *Adv. Mater.* **2018**, *30*, 1801246.
[29] D. Thomson, A. Zilkie, J. E. Bowers, T. Komljenovic, G. T. Reed, L. Vivien, D. Marris-Morini, E. Cassan, L. Virot, J.-M. Fédéli, *J. Opt.* **2016**, *18*, 073003.
[30] G. J. Triggs, Y. Wang, C. P. Reardon, M. Fischer, G. J. Evans, T. F. Krauss, *Optica* **2017**, *4*, 229.
[31] F. Yesilkoy, E. R. Arvelo, Y. Jahani, M. Liu, A. Tittl, V. Cevher, Y. Kivshar, H. Altug, *Nat. Photonics* **2019**, *13*, 390.
[32] Y. Wang, M. A. Ali, E. K. Chow, L. Dong, M. Lu, *Biosens. Bioelectron.* **2018**, *107*, 224.
[33] L. Wang, J. Ren, X. Han, T. Claes, X. Jian, P. Bienstman, R. Baets, M. Zhao, G. Morthier, *IEEE Photonics J.* **2012**, *4*, 920.
[34] Y. Liang, Q. Liu, Z. Wu, G. Morthier, M. Zhao, *Sensors* **2019**, *19*, 181.
[35] M. De Goede, M. Dijkstra, R. Obregón, J. Ramón-Azcón, E. Martínez, L. Padilla, F. Mitjans, S. Garcia-Blanco, *Opt. Express* **2019**, *27*, 18508.
[36] K. Watanabe, Y. Kishi, S. Hachuda, T. Watanabe, M. Sakemoto, Y. Nishijima, T. Baba, *Appl. Phys. Lett.* **2015**, *106*, 021106.
[37] R. Luo, H. Jiang, H. Liang, Y. Chen, Q. Lin, *Opt. Lett.* **2017**, *42*, 1281.
[38] S. K. Arya, C. C. Wong, Y. J. Jeon, T. Bansal, M. K. Park, *Chem. Rev.* **2015**, *115*, 5116.
[39] L. Chrostowski, H. Shoman, M. Hammood, H. Yun, J. Jhoja, E. Luan, S. Lin, A. Mistry, D. Witt, N. A. F. Jaeger, S. Shekhar,

**ADVANCED
SCIENCE NEWS**

www.advancedsciencenews.com

**ADVANCED
MATERIALS
TECHNOLOGIES**

www.advmattechnol.de

H. Jayatilleka, P. Jean, S. B. Villers, J. Cauchon, W. Shi, C. Horvath, J. N. Westwood-Bachman, K. Setzer, M. Aktary, N. S. Patrick, R. J. Bojko, A. Khavasi, X. Wang, T. Ferreira d. Lima, A. N. Tait, P. R. Prucnal, D. E. Hagan, D. Stevanovic, A. P. Knights, *IEEE J. Sel. Top. Quantum Electron.* **2019**, *25*, 1.

[40] K. Shang, S. Pathak, B. Guan, G. Liu, S. Yoo, *Opt. Express* **2015**, *23*, 21334.

[41] D. J. Blumenthal, R. Heideman, D. Geuzebroek, A. Leinse, C. Roeloffzen, *Proc. IEEE* **2018**, *106*, 2209.

[42] M. A. Porcel, A. Hinojosa, H. Jans, A. Stassen, J. Goyvaerts, D. Geuzebroek, M. Geiselmann, C. Dominguez, I. Artundo, *Opt. Laser Technol.* **2019**, *112*, 299.

[43] P. Muñoz, G. Micó, L. Bru, D. Pastor, D. Pérez, J. Doménech, J. Fernández, R. Baños, R. Gargallo, R. Alemany, *Sensors* **2017**, *17*, 2088.

[44] G. Besselink, R. Heideman, E. Schreuder, L. Wevers, F. Falke, H. Van den Vlekkert, *J. Biosens. Bioelectron.* **2016**, *7*, 1000209.

[45] M. H. P. Pfeiffer, C. Herkommer, J. Liu, T. Morais, M. Zervas, M. Geiselmann, T. J. Kippenberg, *IEEE J. Sel. Top. Quantum Electron.* **2018**, *24*, 6101411.

[46] P. Munoz, P. W. van Dijk, D. Geuzebroek, M. Geiselmann, C. Dominguez, A. Stassen, J. D. Doménech, M. Zervas, A. Leinse, C. G. Roeloffzen, *IEEE J. Sel. Top. Quantum Electron.* **2019**, *25*, 8200513.

[47] A. Shakoor, M. Grande, J. Grant, D. R. Cumming, *IEEE Photonics J.* **2017**, *9*, 6800711.

[48] A. Arbabi, L. L. Goddard, *Opt. Lett.* **2013**, *38*, 3878.

[49] D. Psaltis, S. R. Quake, C. Yang, *Nature* **2006**, *442*, 381.

[50] C. Song, S. Tan, *Micromachines* **2017**, *8*, 152.

[51] Y.-F. Chen, L. Jiang, M. Mancuso, A. Jain, V. Oncescu, D. Erickson, *Nanoscale* **2012**, *4*, 4839.

[52] M. Kim, M. Pan, Y. Gai, S. Pang, C. Han, C. Yang, S. K. Y. Tang, *Lab Chip* **2015**, *15*, 1417.

[53] D. Ozcelik, J. W. Parks, T. A. Wall, M. A. Stott, H. Cai, J. W. Parks, A. R. Hawkins, H. Schmidt, *Proc. Natl. Acad. Sci. U. S. A.* **2015**, *112*, 12933.

[54] H. Wan, J. Chen, C. Wan, Q. Zhou, J. Wang, Z. Zhang, *Biomed. Opt. Express* **2019**, *10*, 3929.

[55] Z. Yao, C. C. Kwan, A. W. Poon, *Lab Chip* **2020**, *20*, 601.

[56] K. Ren, J. Zhou, H. Wu, *Acc. Chem. Res.* **2013**, *46*, 2396.

[57] Y. Hwang, O. H. Paydar, R. N. Candler, *Sens. Actuators, A* **2015**, *226*, 137.

[58] Y. Xia, G. M. Whitesides, *Annu. Rev. Mater. Sci.* **1998**, *28*, 153.

[59] D. Carugo, J. Y. Lee, A. Pora, R. J. Browning, L. Capretto, C. Nastruzzi, E. Stride, *Biomed. Microdevices* **2016**, *18*, 4.

[60] G. Comina, A. Suska, D. Filippini, *Lab Chip* **2014**, *14*, 424.

[61] J. Yang, K. Li, L. Zhu, W. Tang, *RSC Adv.* **2017**, *7*, 3313.

[62] A. Lamberti, A. Virga, P. Rivolo, A. Angelini, F. Giorgis, *J. Phys. Chem. B* **2015**, *119*, 8194.

[63] J. Marquez-Garcia, A. S. Cruz-Félix, A. Santiago-Alvarado, J. González-García, in *Material Technologies and Applications to Optics, Structures, Components, and Sub-Systems III* (Eds: J. L. Robichaud, M. Krödel, W. A. Goodman), SPIE, San Diego, CA **2017**, 1037205.

[64] R. Sivakumarasamy, K. Nishiguchi, A. Fujiwara, D. Vuillaume, N. Clement, *Anal. Methods* **2014**, *6*, 97.

[65] J. W. Parks, H. Cai, L. Zempoaltecatl, T. D. Yuzvinsky, K. Leake, A. R. Hawkins, H. Schmidt, *Lab Chip* **2013**, *13*, 4118.

[66] C. Monat, P. Domachuk, B. Eggleton, *Nat. Photonics* **2007**, *1*, 106.

[67] S. Shin, N. Kim, J. W. Hong, *BioChip J.* **2018**, *12*, 123.

[68] J. N. Lee, C. Park, G. M. Whitesides, *Anal. Chem.* **2003**, *75*, 6544.

[69] D. Kim, A. E. Herr, *Biomicrofluidics* **2013**, *7*, 041501.

[70] H. Long, C. Lai, C.-K. Chung, *Surf. Coat. Technol.* **2017**, *320*, 315.

[71] J. Hu, V. Tarasov, A. Agarwal, L. Kimerling, N. Carlie, L. Petit, K. Richardson, *Opt. Express* **2007**, *15*, 2307.

[72] V. V. Parsi Sreenivas, A. Winkler, S. Harazim, O. G. Schmidt, *J. Vac. Sci. Technol. B* **2018**, *36*, 051601.

[73] E. Luan, H. Shoman, D. Ratner, K. Cheung, L. Chrostowski, *Sensors* **2018**, *18*, 3519.

[74] M. Hashimoto, R. Langer, D. S. Kohane, *Lab Chip* **2013**, *13*, 252.

[75] S. H. Kim, Y. Yang, M. Kim, S. W. Nam, K. M. Lee, N. Y. Lee, Y. S. Kim, S. Park, *Adv. Funct. Mater.* **2007**, *17*, 3493.

[76] T. Lipka, L. Moldenhauer, L. Wahn, H. Trieu, *Opt. Lett.* **2017**, *42*, 1084.

[77] J. Wang, A. W. Poon, *Lab Chip* **2014**, *14*, 1426.

[78] M.-J. Bañuls, R. Puchades, Á. Maquieira, *Anal. Chim. Acta* **2013**, *777*, 1.

[79] H. K. Hunt, A. M. Armani, *IEEE J. Sel. Top. Quantum Electron.* **2013**, *20*, 121.

[80] N. Aissaoui, L. Bergaoui, J. Landoulsi, J.-F. Lambert, S. Boujday, *Langmuir* **2012**, *28*, 656.

[81] J. I. A. Rashid, N. A. Yusof, *Sens. Bio-Sensing Res.* **2017**, *16*, 19.

[82] C. S. Huertas, O. Calvo Lozano, A. Mitchell, L. M. Lechuga, *Front. Chem.* **2019**, *7*, 724.

[83] N. A. Lapin, Y. J. Chabal, *J. Phys. Chem. B* **2009**, *113*, 8776.

[84] K. De Vos, I. Bartolozzi, E. Schacht, P. Bienstman, R. Baets, *Opt. Express* **2007**, *15*, 7610.

[85] Z. Yao, K. Wu, B. X. Tan, J. Wang, Y. Li, Y. Zhang, A. W. Poon, *IEEE J. Sel. Top. Quantum Electron.* **2018**, *24*, 5900324.

[86] R. Kou, Y. Kobayashi, S. Inoue, T. Tsuchizawa, Y. Ueno, S. Suzuki, H. Hibino, T. Yamamoto, H. Nakajima, K. Yamada, *Opt. Express* **2019**, *27*, 32058.

[87] D. Amarie, J. Glazier, *Sensors* **2012**, *12*, 17262.

[88] H. Vaisocherová, E. Brynda, J. Homola, *Anal. Bioanal. Chem.* **2015**, *407*, 3927.

[89] Y. Jeyachandran, J. Mielczarski, E. Mielczarski, B. Rai, *J. Colloid Interface Sci.* **2010**, *341*, 136.

[90] H. Mukundan, H. Xie, A. S. Anderson, W. K. Grace, J. E. Shively, B. I. Swanson, *Bioconjugate Chem.* **2009**, *20*, 222.

[91] M. V. Riquelme, H. Zhao, V. Srinivasaraghavan, A. Pruden, P. Vikesland, M. Agah, *Sens. Bio-Sensing Res.* **2016**, *8*, 47.

[92] M. S. Luchansky, A. L. Washburn, M. S. McClellan, R. C. Bailey, *Lab Chip* **2011**, *11*, 2042.

[93] A. Psarouli, A. Botsialas, A. Salapatas, G. Stefanitsis, D. Nikita, G. Jobst, N. Chaniotakis, D. Goustouridis, E. Makarona, P. S. Petrou, *Talanta* **2017**, *165*, 458.

[94] D. Martens, P. Ramirez-Priego, M. S. Murib, A. A. Elamin, A. B. González-Guerrero, M. Stehr, F. Jonas, B. Anton, N. Hlawatsch, P. Soetaert, *Anal. Methods* **2018**, *10*, 3066.

[95] M. S. Luchansky, R. C. Bailey, *J. Am. Chem. Soc.* **2011**, *133*, 20500.

[96] O. Scheler, J. T. Kindt, A. J. Qavi, L. Kaplinski, B. Glynn, T. Barry, A. Kurg, R. C. Bailey, *Biosens. Bioelectron.* **2012**, *36*, 56.

[97] P. Ramirez-Priego, D. Martens, A. A. Elamin, P. Soetaert, W. Van Roy, R. Vos, B. Anton, R. Bockstaele, H. Becker, M. Singh, *ACS Sens.* **2018**, *3*, 2079.

[98] Q. Liu, B. K. L. Lim, S. Y. Lim, W. Y. Tang, Z. Gu, J. Chung, M. K. Park, T. Barkham, *Sens. Actuators, B* **2018**, *255*, 1595.

[99] S. Wu, S. Guo, W. Wang, J. Zhou, Q. Zhang, *Rev. Sci. Instrum.* **2019**, *90*, 035004.

[100] S. Chakravarty, W.-C. Lai, Y. Zou, H. A. Drabkin, R. M. Gemmill, G. R. Simon, S. H. Chin, R. T. Chen, *Biosens. Bioelectron.* **2013**, *43*, 50.

[101] M. Fukuyama, M. Nishida, Y. Abe, Y. Amemiya, T. Ikeda, A. Kuroda, S. Yokoyama, *Jpn. J. Appl. Phys.* **2011**, *50*, 04DL07.

[102] A. L. Washburn, L. C. Gunn, R. C. Bailey, *Anal. Chem.* **2009**, *81*, 9499.

[103] C.-J. Yang, N. Tang, H. Yan, S. Chakravarty, D. Li, R. T. Chen, presented at *Conf. on Lasers and Electro-Optics*, San Jose, CA May **2015**.

[104] Q. Liu, Y. Shin, J. S. Kee, K. W. Kim, S. R. M. Rafei, A. P. Perera, X. Tu, G.-Q. Lo, E. Ricci, M. Colombel, *Biosens. Bioelectron.* **2015**, *71*, 365.

**ADVANCED
SCIENCE NEWS**

www.advancedsciencenews.com

**ADVANCED
MATERIALS
TECHNOLOGIES**

www.advmattechnol.de

[105] K. De Vos, J. Girones, T. Claes, Y. De Koninck, S. Popelka, E. Schacht, R. Baets, P. Bienstman, *IEEE Photonics J.* **2009**, *1*, 225.

[106] M.-C. Estevez, M. Alvarez, L. M. Lechuga, *Laser Photonics Rev.* **2012**, *6*, 463.

[107] A. Fernández Gavela, D. Grajales García, J. Ramirez, L. Lechuga, *Sensors* **2016**, *16*, 285.

[108] H. Mukundan, A. Anderson, W. K. Grace, K. Grace, N. Hartman, J. Martinez, B. Swanson, *Sensors* **2009**, *9*, 5783.

[109] A. B. González-Guerrero, J. Maldonado, S. Herranz, L. M. Lechuga, *Anal. Methods* **2016**, *8*, 8380.

[110] P. Kozma, F. Kehl, E. Ehrentreich-Förster, C. Stamm, F. F. Bier, *Biosens. Bioelectron.* **2014**, *58*, 287.

[111] R. Heideman, R. Kooyman, J. Greve, *Sens. Actuators, B* **1991**, *4*, 297.

[112] A. Ymeti, J. Greve, P. V. Lambeck, T. Wink, S. W. van Hövell, T. A. Beumer, R. R. Wijn, R. G. Heideman, V. Subramaniam, J. S. Kanger, *Nano Lett.* **2007**, *7*, 394.

[113] A. Densmore, M. Vachon, D.-X. Xu, S. Janz, R. Ma, Y.-H. Li, G. Lopinski, A. Delâge, J. Lapointe, C. Luebbert, *Opt. Lett.* **2009**, *34*, 3598.

[114] J. Xu, D. Suarez, D. S. Gottfried, *Anal. Bioanal. Chem.* **2007**, *389*, 1193.

[115] C. S. Huertas, D. Fariña, L. M. Lechuga, *ACS Sens.* **2016**, *1*, 748.

[116] K. Uchiyamada, K. Okubo, M. Yokokawa, E. Carlen, K. Asakawa, H. Suzuki, *Opt. Express* **2015**, *23*, 17156.

[117] E. Melnik, P. Muellner, G. C. Mutinati, G. Koppitsch, F. Schrank, R. Hainberger, M. Laemmerhofer, *Sens. Actuators, B* **2016**, *236*, 1061.

[118] K. Misiakos, I. Raptis, A. Salapatas, E. Makarona, A. Botsialas, M. Hoekman, R. Stoffer, G. Jobst, *Opt. Express* **2014**, *22*, 8856.

[119] J. Maldonado, A. B. González-Guerrero, C. Domínguez, L. M. Lechuga, *Biosens. Bioelectron.* **2016**, *85*, 310.

[120] C. S. Huertas, S. Domínguez-Zotes, L. M. Lechuga, *Sci. Rep.* **2017**, *7*, 41368.

[121] J. Maldonado, M.-C. Estévez, A. Fernández-Gavela, J. J. González-López, A. B. González-Guerrero, L. M. Lechuga, *Analyst* **2020**, *145*, 497.

[122] A. B. González-Guerrero, J. Maldonado, S. Dante, D. Grajales, L. M. Lechuga, *J. Biophotonics* **2017**, *10*, 61.

[123] K. J. Vahala, *Nature* **2003**, *424*, 839.

[124] F. Vollmer, D. Braun, A. Libchaber, M. Khoshsima, I. Teraoka, S. Arnold, *Appl. Phys. Lett.* **2002**, *80*, 4057.

[125] H. Jeong, S. Lee, G. Y. Sung, J. H. Shin, *IEEE Photonics Technol. Lett.* **2010**, *23*, 88.

[126] G. Kim, J. H. Shin, *IEEE Photonics Technol. Lett.* **2016**, *28*, 2331.

[127] P. Steglich, M. Hülsemann, B. Dietzel, A. Mai, *Molecules* **2019**, *24*, 519.

[128] J. H. Wade, R. C. Bailey, *Annu. Rev. Anal. Chem.* **2016**, *9*, 1.

[129] S. Feng, T. Lei, H. Chen, H. Cai, X. Luo, A. W. Poon, *Laser Photonics Rev.* **2012**, *6*, 145.

[130] A. L. Washburn, M. S. Luchansky, A. L. Bowman, R. C. Bailey, *Anal. Chem.* **2010**, *82*, 69.

[131] M. Iqbal, M. A. Gleeson, B. Spaugh, F. Tybor, W. G. Gunn, M. Hochberg, T. Baehr-Jones, R. C. Bailey, L. C. Gunn, *IEEE J. Sel. Top. Quantum Electron.* **2010**, *16*, 654.

[132] J. T. Kirk, G. E. Fridley, J. W. Chamberlain, E. D. Christensen, M. Hochberg, D. M. Ratner, *Lab Chip* **2011**, *11*, 1372.

[133] F. Ghasemi, E. S. Hosseini, X. Song, D. S. Gottfried, M. Chamanzar, M. Raeiszadeh, R. D. Cummings, A. A. Eftekhar, A. Adibi, *Biosens. Bioelectron.* **2016**, *80*, 682.

[134] J. Juan-Colás, A. Parkin, K. E. Dunn, M. G. Scullion, T. F. Krauss, S. D. Johnson, *Nat. Commun.* **2016**, *7*, 12769.

[135] J. Juan-Colás, S. Johnson, T. Krauss, *Sensors* **2017**, *17*, 2047.

[136] J. Juan-Colás, T. F. Krauss, S. D. Johnson, *ACS Photonics* **2017**, *4*, 2320.

[137] Y.-n. Zhang, Y. Zhao, T. Zhou, Q. Wu, *Lab Chip* **2018**, *18*, 57.

[138] H. Inan, M. Poyraz, F. Inci, M. A. Lifson, M. Baday, B. T. Cunningham, U. Demirci, *Chem. Soc. Rev.* **2017**, *46*, 366.

[139] S. Chakravarty, J. Topol'ančik, P. Bhattacharya, S. Chakrabarti, Y. Kang, M. Meyerhoff, *Opt. Lett.* **2005**, *30*, 2578.

[140] S. Chakravarty, X. Chen, N. Tang, W.-C. Lai, Y. Zou, H. Yan, R. T. Chen, *Front. Optoelectron.* **2016**, *9*, 206.

[141] M. Lee, P. M. Fauchet, *Opt. Express* **2007**, *15*, 4530.

[142] H. Yan, C.-J. Yang, N. Tang, Y. Zou, S. Chakravarty, A. Roth, R. T. Chen, *IEEE Sens. J.* **2017**, *17*, 5915.

[143] D. Yang, S. Kita, F. Liang, C. Wang, H. Tian, Y. Ji, M. Lončar, Q. Quan, *Appl. Phys. Lett.* **2014**, *105*, 063118.

[144] M. R. Lee, P. M. Fauchet, *Opt. Lett.* **2007**, *32*, 3284.

[145] J. E. Baker, R. Sriram, B. L. Miller, *Lab Chip* **2017**, *17*, 1570.

[146] C. Wang, Q. Quan, S. Kita, Y. Li, M. Lončar, *Appl. Phys. Lett.* **2015**, *106*, 261105.

[147] J. Milvich, D. Kohler, W. Freude, C. Koos, *Opt. Express* **2018**, *26*, 19885.

[148] S. TalebiFard, S. Schmidt, W. Shi, W. Wu, N. A. Jaeger, E. Kwok, D. M. Ratner, L. Chrostowski, *Biomed. Opt. Express* **2017**, *8*, 500.

[149] T. Baehr-Jones, M. Hochberg, C. Walker, A. Scherer, *Appl. Phys. Lett.* **2005**, *86*, 081101.

[150] S. Lee, S. C. Eom, J. S. Chang, C. Huh, G. Y. Sung, J. H. Shin, *Opt. Express* **2010**, *18*, 20638.

[151] M. Scullion, A. Di Falco, T. Krauss, *Biosens. Bioelectron.* **2011**, *27*, 101.

[152] C. F. Carlborg, K. B. Gylfason, A. Kaźmierczak, F. Dortu, M. B. Polo, A. M. Catala, G. M. Kresbach, H. Sohlström, T. Moh, L. Vivien, *Lab Chip* **2010**, *10*, 281.

[153] M. Scullion, T. Krauss, A. Di Falco, *Sensors* **2013**, *13*, 3675.

[154] J. Zhou, H. Tian, L. Huang, Z. Fu, F. Sun, Y. Ji, *IEEE Photonics Technol. Lett.* **2016**, *29*, 1281.

[155] S. T. Fard, V. Donzella, S. A. Schmidt, J. Flueckiger, S. M. Grist, P. T. Fard, Y. Wu, R. J. Bojko, E. Kwok, N. A. Jaeger, *Opt. Express* **2014**, *22*, 14166.

[156] G. Gaur, S. Hu, R. L. Mernaugh, I. I. Kravchenko, S. T. Retterer, S. M. Weiss, *Sens. Actuators, B* **2018**, *275*, 394.

[157] A. Jane, R. Dronov, A. Hodges, N. H. Voelcker, *Trends Biotechnol.* **2009**, *27*, 230.

[158] G. A. Rodriguez, P. Markov, A. P. Cartwright, M. H. Choudhury, F. O. Afzal, T. Cao, S. I. Halimi, S. T. Retterer, I. I. Kravchenko, S. M. Weiss, *Opt. Express* **2019**, *27*, 9536.

[159] W. Lee, H. Li, J. D. Suter, K. Reddy, Y. Sun, X. Fan, *Appl. Phys. Lett.* **2011**, *98*, 061103.

[160] Y. Wang, C. Xu, M. Jiang, J. Li, J. Dai, J. Lu, P. Li, *Nanoscale* **2016**, *8*, 16631.

[161] Y. Chang, B. Dong, Y. Ma, J. Wei, Z. Ren, C. Lee, *Opt. Express* **2020**, *28*, 6251.

[162] D. Dai, *Opt. Express* **2009**, *17*, 23817.

[163] X. Jiang, J. Ye, J. Zou, M. Li, J.-J. He, *Opt. Lett.* **2013**, *38*, 1349.

[164] Y. Chen, F. Yu, C. Yang, J. Song, L. Tang, M. Li, J.-J. He, *Opt. Commun.* **2015**, *344*, 129.

[165] K. Qin, S. Hu, S. T. Retterer, I. I. Kravchenko, S. M. Weiss, *Opt. Lett.* **2016**, *41*, 753.

[166] K. Uchiyamada, K. Okubo, K. Asakawa, Y. Kamon, Y. Kitayama, T. Takeuchi, H. Suzuki, *Adv. Mater. Technol.* **2019**, *4*, 1800533.

[167] J. Y. Lee, P. M. Fauchet, *Opt. Lett.* **2012**, *37*, 58.

[168] S. M. Lo, S. Hu, G. Gaur, Y. Kostoulas, S. M. Weiss, P. M. Fauchet, *Opt. Express* **2017**, *25*, 7046.

[169] R. Halir, A. Ortega-Moñux, D. Benedikovic, G. Z. Mashanovich, J. G. Wangüemert-Pérez, J. H. Schmid, Í. Molina-Fernández, P. Cheben, *Proc. IEEE* **2018**, *106*, 2144.

[170] L. Huang, H. Yan, X. Xu, S. Chakravarty, N. Tang, H. Tian, R. T. Chen, *Opt. Express* **2017**, *25*, 10527.

[171] V. Donzella, A. Sherwali, J. Flueckiger, S. M. Grist, S. T. Fard, L. Chrostowski, *Opt. Express* **2015**, *23*, 4791.

[172] J. G. Wangüemert-Pérez, A. Hadij-ElHouati, A. Sánchez-Postigo, J. Leuermann, D.-X. Xu, P. Cheben, A. Ortega-Moñux, R. Halir, Í. Molina-Fernández, *Opt. Laser Technol.* **2019**, *109*, 437.

[173] L. Zhang, D. Dai, *IEEE Photonics Technol. Lett.* **2019**, *31*, 1209.

[174] J. Flueckiger, S. Schmidt, V. Donzella, A. Sherwali, D. M. Ratner, L. Chrostowski, K. C. Cheung, *Opt. Express* **2016**, *24*, 15672.

[175] E. Luan, K. M. Awan, K. C. Cheung, L. Chrostowski, *Opt. Lett.* **2019**, *44*, 5981.

[176] Z. Wang, X. Xu, D. Fan, Y. Wang, R. T. Chen, *Opt. Lett.* **2016**, *41*, 3375.

[177] C.-W. Chang, X. Xu, S. Chakravarty, H.-C. Huang, L.-W. Tu, Q. Y. Chen, H. Dalir, M. A. Krainak, R. T. Chen, *Biosens. Bioelectron.* **2019**, *141*, 111396.

[178] E. Luan, H. Yun, L. Laplatine, J. Flueckiger, Y. Dattner, D. Ratner, K. Cheung, L. Chrostowski, in *Integrated Optics: Devices, Materials, and Technologies XXII* (Eds: S. M. García-Blanco, P. Cheben), SPIE, San Francisco, CA **2018**, p. 105350H.

[179] E. Luan, H. Yun, L. Laplatine, Y. Dattner, D. M. Ratner, K. C. Cheung, L. Chrostowski, *IEEE J. Sel. Top. Quantum Electron.* **2019**, *25*, 7300211.

[180] E. Luan, H. Yun, M. Ma, D. M. Ratner, K. C. Cheung, L. Chrostowski, *Biomed. Opt. Express* **2019**, *10*, 4825.

[181] M. Odeh, K. Twayana, K. Sloyan, J. E. Villegas, S. Chandran, M. S. Dahlem, *IEEE Photonics J.* **2019**, *11*, 1.

[182] T. Claes, W. Bogaerts, P. Bienstman, *Opt. Lett.* **2011**, *36*, 3320.

[183] J. Song, X. Luo, X. Tu, M. K. Park, J. S. Kee, H. Zhang, M. Yu, G.-Q. Lo, D.-L. Kwong, *Opt. Express* **2012**, *20*, 4189.

[184] P. Moock, L. Kasper, M. Jäger, D. Stolarek, H. Richter, J. Bruns, K. Petermann, *Opt. Express* **2018**, *26*, 22356.

[185] J. Wang, Z. Yao, T. Lei, A. W. Poon, *Sci. Rep.* **2015**, *4*, 7528.

[186] J. Wang, Z. Yao, A. W. Poon, *Front. Mater.* **2015**, *2*, 34.

[187] J. Wang, Z. Yao, A. W. Poon, in *Integrated Optics: Devices, Materials, and Technologies XX* (Eds: J.-E. Broquin, G. N. Conti), Proc. SPIE, San Francisco, CA **2016**, p. 975014.

[188] M. Angelopoulou, S. Kakabakos, P. Petrou, *Chemosensors* **2018**, *6*, 52.

[189] C. L. Arce, D. Witters, R. Puers, J. Lammertyn, P. Bienstman, *Anal. Bioanal. Chem.* **2012**, *404*, 2887.

[190] A. Psarouli, A. Salapatas, A. Botsialas, P. Petrou, I. Raptis, E. Makarona, G. Jobst, K. Tukkiniemi, M. Sopanen, R. Stoffer, *Sci. Rep.* **2015**, *5*, 17600.

[191] S. Geidel, S. Peransi Llopis, M. Rodrigo, G. de Diego-Castilla, A. Sousa, J. Nestler, T. Otto, T. Gessner, V. Parro, *Micromachines* **2016**, *7*, 153.

[192] C. Szydzik, A. Gavela, S. Herranz, J. Roccisano, M. Knoerzer, P. Thurgood, K. Khoshmanesh, A. Mitchell, L. M. Lechuga, *Lab Chip* **2017**, *17*, 2793.

[193] L. Laplatine, E. Luan, K. Cheung, D. M. Ratner, Y. Dattner, L. Chrostowski, *Sens. Actuators, B* **2018**, *273*, 1610.

[194] K. Misiakos, E. Makarona, M. Hoekman, R. Fyrogenis, K. Tukkiniemi, G. Jobst, P. S. Petrou, S. E. Kakabakos, A. Salapatas, D. Goustouridis, M. Harjanne, P. Heimala, I. Raptis, *ACS Photonics* **2019**, *6*, 1694.

[195] W. Jung, J. Han, J.-W. Choi, C. H. Ahn, *Microelectron. Eng.* **2015**, *132*, 46.

[196] L. Luan, R. D. Evans, N. M. Jokerst, R. B. Fair, *IEEE Sens. J.* **2008**, *8*, 628.

[197] L. Luan, M. W. Royal, R. Evans, R. B. Fair, N. M. Jokerst, *IEEE Sens. J.* **2011**, *12*, 1794.

[198] S. F. Wondimu, S. von der Ecken, R. Ahrens, W. Freude, A. E. Guber, C. Koos, *Lab Chip* **2017**, *17*, 1740.

[199] A. Shakoor, B. C. Cheah, D. Hao, M. Al-Rawhani, B. Nagy, J. Grant, C. Dale, N. Keegan, C. McNeil, D. R. Cumming, *ACS Photonics* **2016**, *3*, 1926.

[200] A. Shakoor, J. Grant, M. Grande, D. Cumming, *Sensors* **2019**, *19*, 1715.

[201] L. Augel, F. Berkmann, D. Latta, I. A. Fischer, S. Bechler, Y. Elogail, K. Kostecki, K. Potje-Kamloth, J. Schulze, *Microfluid. Nanofluid.* **2017**, *21*, 169.

[202] M. Anastasopoulou, A. Malainou, A. Salapatas, N. Chronis, I. Raptis, K. Misiakos, *Sens. Actuators, B* **2018**, *256*, 304.

[203] G. Quaranta, G. Basset, O. J. Martin, B. Gallinet, *Laser Photonics Rev.* **2018**, *12*, 1800017.

[204] J. Vörös, J. Ramsden, G. Csucs, I. Szendrő, M. De Paul, M. Textor, N. Spencer, *Biomaterials* **2002**, *23*, 3699.

[205] D. Patko, K. Cottier, A. Hamori, R. Horvath, *Opt. Express* **2012**, *20*, 23162.

[206] D. Patko, B. Gyorgy, A. Nemeth, K. Szabó-Taylor, A. Kittel, E. I. Buzás, R. Horvath, *Sens. Actuators, B* **2013**, *188*, 697.

[207] X. Wei, S. M. Weiss, *Opt. Express* **2011**, *19*, 11330.

[208] S. Mudumba, S. de Alba, R. Romero, C. Cherwien, A. Wu, J. Wang, M. A. Gleeson, M. Iqbal, R. W. Burlingame, *J. Immunol. Methods* **2017**, *448*, 34.

[209] E. H. Mordan, J. H. Wade, Z. S. Wiersma, E. Pearce, T. O. Pangburn, A. W. deGroot, D. M. Meunier, R. C. Bailey, *Anal. Chem.* **2019**, *91*, 1011.

[210] M. Miyara, J.-L. Charuel, S. Mudumba, A. Wu, P. Ghillani-Dalbin, Z. Amoura, R. W. Burlingame, L. Musset, *PLoS One* **2018**, *13*, e0202736.

[211] V. R. Dantham, S. Holler, C. Barbre, D. Keng, V. Kolchenko, S. Arnold, *Nano Lett.* **2013**, *13*, 3347.

[212] E. Kim, M. D. Baaske, F. Vollmer, *Lab Chip* **2017**, *17*, 1190.

[213] X. Jiang, A. J. Qavi, S. H. Huang, L. Yang, *arXiv:1805.00062*, **2018**.

[214] Y. Zhi, X. C. Yu, Q. Gong, L. Yang, Y. F. Xiao, *Adv. Mater.* **2017**, *29*, 1604920.

[215] L. He, Ş. K. Özdemir, J. Zhu, W. Kim, L. Yang, *Nat. Nanotechnol.* **2011**, *6*, 428.

[216] F. Vollmer, S. Arnold, *Nat. Methods* **2008**, *5*, 591.

[217] X. Ji, F. A. Barbosa, S. P. Roberts, A. Dutt, J. Cardenas, Y. Okawachi, A. Bryant, A. L. Gaeta, M. Lipson, *Optica* **2017**, *4*, 619.

[218] D. T. Spencer, J. F. Bauters, M. J. Heck, J. E. Bowers, *Optica* **2014**, *1*, 153.

[219] K. Y. Yang, D. Y. Oh, S. H. Lee, Q.-F. Yang, X. Yi, B. Shen, H. Wang, K. Vahala, *Nat. Photonics* **2018**, *12*, 297.

[220] W. Chen, Ş. K. Özdemir, G. Zhao, J. Wiersig, L. Yang, *Nature* **2017**, *548*, 192.

[221] E. Chatzianagnostou, A. Manolis, G. Dabos, A. Ketzaki, A. Miliou, N. Pleros, L. Markey, J.-C. Weeber, A. Dereux, B. Chmielak, *ACS Photonics* **2019**, *6*, 1664.

[222] J. Lee, J. Song, G. Y. Sung, J. H. Shin, *Nano Lett.* **2014**, *14*, 5533.

[223] X. Yang, A. Ishikawa, X. Yin, X. Zhang, *ACS Nano* **2011**, *5*, 2831.

[224] J. Xavier, S. Vincent, F. Meder, F. Vollmer, *Nanophotonics* **2018**, *7*, 1.

[225] M. D. Baaske, M. R. Foreman, F. Vollmer, *Nat. Nanotechnol.* **2014**, *9*, 933.

[226] S. Frustaci, F. Vollmer, *Curr. Opin. Chem. Biol.* **2019**, *51*, 66.

[227] T. Zhang, S. Callard, C. Jamois, C. Chevalier, D. Feng, A. Belarouci, *Nanotechnology* **2014**, *25*, 315201.

[228] D. Conteduca, C. Reardon, M. G. Scullion, F. Dell'Olio, M. N. Armenise, T. F. Krauss, C. Ciminelli, *APL Photonics* **2017**, *2*, 086101.

[229] J. Losada, A. Raza, S. Clemmen, A. Serrano, A. Griol, R. Baets, A. Martínez, *IEEE J. Sel. Top. Quantum Electron.* **2019**, *25*, 4600806.

[230] T. Ma, J. Yuan, L. Sun, F. Li, Z. Kang, B. Yan, X. Sang, K. Wang, Q. Wu, H. Liu, *Plasmonics* **2017**, *12*, 1417.

[231] F. Dell'Olio, D. Conteduca, M. De Palo, C. Ciminelli, *Sensors* **2017**, *17*, 1810.

[232] A. B. Ayoub, D. Ji, Q. Gan, M. A. Swillam, *Opt. Commun.* **2018**, *427*, 319.

[233] E. Kim, M. D. Baaske, F. Vollmer, *Adv. Mater.* **2016**, *28*, 9941.

[234] A. Aiello, P. Banzer, M. Neugebauer, G. Leuchs, *Nat. Photonics* **2015**, *9*, 789.

**ADVANCED
SCIENCE NEWS**

www.advancedsciencenews.com

**ADVANCED
MATERIALS
TECHNOLOGIES**

www.advmattechnol.de

[235] L. Ma, S. Li, V. M. Fomin, M. Hentschel, J. B. Götte, Y. Yin, M. Jorgensen, O. G. Schmidt, *Nat. Commun.* **2016**, *7*, 10983.

[236] A. Madani, M. Kleinert, D. Stolarek, L. Zimmermann, L. Ma, O. G. Schmidt, *Opt. Lett.* **2015**, *40*, 3826.

[237] X. Yu, E. Arbabi, L. L. Goddard, X. Li, X. Chen, *Appl. Phys. Lett.* **2015**, *107*, 031102.

[238] A. Madani, S. M. Harazim, V. A. B. Quiñones, M. Kleinert, A. Finn, E. S. G. Naz, L. Ma, O. G. Schmidt, *Opt. Lett.* **2017**, *42*, 486.

[239] J. Wang, Y. Yin, Q. Hao, Y. Zhang, L. Ma, O. G. Schmidt, *Adv. Opt. Mater.* **2018**, *6*, 1700842.

[240] J. Wang, D. Karnaushenko, M. Medina-Sanchez, Y. Yin, L. Ma, O. G. Schmidt, *ACS Sens.* **2019**, *4*, 1476.

[241] Z. Li, C. Zhu, Z. Guo, B. Wang, X. Wu, Y. Fei, *Micromachines* **2018**, *9*, 274.

[242] S. M. Harazim, V. A. B. Quiñones, S. Kiravittaya, S. Sanchez, O. G. Schmidt, *Lab Chip* **2012**, *12*, 2649.

[243] S. Miao, D. Chen, A. Madani, M. R. Jorgensen, V. A. Bolaños Quiñones, L. Ma, S. G. Hickey, A. Eychmüller, O. G. Schmidt, *Adv. Opt. Mater.* **2015**, *3*, 187.

[244] Y. Yin, J. Wang, X. Wang, S. Li, M. R. Jorgensen, J. Ren, S. Meng, L. Ma, O. G. Schmidt, *Sci. Adv.* **2019**, *5*, eaax6973.

[245] Y. Yin, J. Pang, J. Wang, X. Lu, Q. Hao, E. Saei Ghareh Naz, X. Zhou, L. Ma, O. G. Schmidt, *ACS Appl. Mater. Interfaces* **2019**, *11*, 15891.

[246] C. S. Bausch, C. Heyn, W. Hansen, I. M. Wolf, B.-P. Diercks, A. H. Guse, R. H. Blick, *Sci. Rep.* **2017**, *7*, 41584.

[247] M. Medina-Sánchez, B. Ibarlucea, N. Pérez, D. D. Karnaushenko, S. M. Weiz, L. Baraban, G. Cuniberti, O. G. Schmidt, *Nano Lett.* **2016**, *16*, 4288.

[248] X. Xu, A. Akay, H. Wei, S. Wang, B. Pingguan-Murphy, B.-E. Erlandsson, X. Li, W. Lee, J. Hu, L. Wang, *Proc. IEEE* **2015**, *103*, 236.

[249] I. Hernández-Neuta, F. Neumann, J. Brightmeyer, T. Ba Tis, N. Madaboosi, Q. Wei, A. Ozcan, M. Nilsson, *J. Intern. Med.* **2019**, *285*, 19.

[250] S. Kanchi, M. I. Sabela, P. S. Mdluli, K. Bisetty, *Biosens. Bioelectron.* **2018**, *102*, 136.

[251] Z. Geng, X. Zhang, Z. Fan, X. Lv, Y. Su, H. Chen, *Sensors* **2017**, *17*, 2449.

[252] C. Lertvachirapaiboon, A. Baba, K. Shinbo, K. Kato, *Anal. Methods* **2018**, *10*, 4732.

[253] X. Wang, T.-W. Chang, G. Lin, M. R. Gartia, G. L. Liu, *Anal. Chem.* **2017**, *89*, 611.

[254] J. Guo, *Anal. Chem.* **2016**, *88*, 11986.

[255] H. Guner, E. Ozgur, G. Kokturk, M. Celik, E. Esen, A. E. Topal, S. Ayas, Y. Uludag, C. Elbuken, A. Dana, *Sens. Actuators, B* **2017**, *239*, 571.

[256] J. Zhang, I. Khan, Q. Zhang, X. Liu, J. Dostalek, B. Liedberg, Y. Wang, *Biosens. Bioelectron.* **2018**, *99*, 312.

[257] M. Schäfer, V. Bräuler, R. Ulber, *Sens. Actuators, B* **2018**, *255*, 1902.

[258] L.-J. Wang, Y.-C. Chang, R. Sun, L. Li, *Biosens. Bioelectron.* **2017**, *87*, 686.

[259] A. Kenaan, K. Li, I. Barth, S. Johnson, J. Song, T. F. J. B. Krauss, *Biosens. Bioelectron.* **2020**, *153*, 112047.

[260] R. P. de Campos, D. G. Rackus, R. Shih, C. Zhao, X. Liu, A. R. Wheeler, *Anal. Chem.* **2019**, *91*, 2506.

[261] A. F. Coskun, S. N. Topkaya, A. K. Yetisen, A. E. Cetin, *Adv. Opt. Mater.* **2019**, *7*, 1801109.

1901138 (24 of 24)